Revised Eburnean geodynamic evolution of the gold-rich southern Ashanti Belt, Ghana, with new field and geophysical evidence of pre-Tarkwaian deformations

Stéphane Perrouty [a,b,*], Laurent Aillères [b], Mark W. Jessell [c], Lenka Baratoux [c], Yan Bourassa [d], Brenton Crawford [b]

[a] Université de Toulouse; UPS (SVT-OMP), GET, 14 Av Edouard Belin, F-31400 Toulouse, France
[b] Monash University, School of Geosciences, Wellington Road, Clayton, Vic 3800, Australia
[c] Institut de Recherche pour le Développement, UR 234, GET, 14 Av, Edouard Belin, F-31400 Toulouse, France
[d] Golden Star Resources Ltd., 10901 W. Toller Drive, Suite 300, Littleton, CO, United States

ABSTRACT

Integration of regional geophysical datasets and detailed field observations provide new insights into the paleoproterozoic structural evolution of southwestern Ghana. The study area is dominated by three metavolcanic and metasedimentary packages known as the Sefwi Group, the Kumasi Group (Birimian) and the Tarkwa Group (Tarkwaian) that were intruded by abundant TTG granitoids during the Eoeburnean and Eburnean phases of an event termed the "Eburnean Orogeny". This study identifies an Eoeburnean (pre-Tarkwaian) deformation event (D1) that produced significant deformation in the Sefwi Group metavolcanics. D1 is associated with N-S shortening manifested as regional scale folding in the southern Ashanti belt. D1 synorogenic granitoids were intruded between 2187 Ma and 2158 Ma under greenschist metamorphic condition. Syn-D1 gold mineralisation associated with quartz veining could be the original source of Tarkwaian paleo-placers and/or remobilised gold concentrations along major shear zones.

D2 represents an extensional phase associated with the Kumasi Group sedimentation (2154–2125 Ma) which could be related to activation of major structures such as the Ashanti Fault as low angle detachments that controlled the deposition of the Kumasi Group and the opening of the Kumasi and Akyem Basin. The Tarkwa Group (2107–2097 Ma) unconformably overlies the Birimian Supergroups and was deposited in response to D3 shortening. D3 resulted in the inversion of syn-D2 detachments faults within the Ashanti Belt. NW-SE D3 shortening produced regional scale folding within the Birimian and the Tarkwaian metasediments. D4 deformation corresponds with sinistral reactivation of D3 thrust faults, and is locally associated with macro-scale folding at Obuasi and Wassa gold mines. By the end of D4, the regional scale architecture was built and was only slightly modified by the two last events. D5 postdates the Eburnean metamorphic peak and corresponds to open recumbent folds associated with a subhorizontal crenulation cleavage. D6 is present as a subvertical crenulation cleavage and reverse faults associated with NE-SW shortening.

1. Introduction

The Ashanti greenstone belt in the Western Region of Ghana hosts numerous hydrothermal gold deposits (e.g. Obuasi, 60 Moz) and older placer deposits (e.g. Tarkwa, 41 Moz) that were created and deformed during the Eburnean orogeny (Bonhomme, 1962). The presence of massive gold placers that predate all known hydrothermal deposits, suggests an early phase of gold mineralisation and subsequent deformation in the Ashanti Belt. Characterising this early event is essential for understanding the tectonic evolution and geological context for gold mineralisation in the south-west Ghana. This region is composed primarily of paleoproterozoic metavolcanic and metasedimentary rocks that are divided into the Birimian Supergroup (Sefwi and Kumasi Groups) and the Tarkwa Group, that are both intruded by abundant granitoids (Fig. 1).

Allibone et al. (2002a) separated the Paleoproterozoic Eburnean orogeny into two distinct phases known as Eburnean I and II. Their Eburnean I event predates the deposition of Tarkwaian sediments and is associated with a major period of magmatism and metamorphism in the Sefwi Group basement. Their Eburnean II event is associated with significant post-Tarkwaian deformation

* Corresponding author at: GET, Observatoire Midi-Pyrénées, 14 Av Edouard Belin, F-31400 Toulouse, France. Tel.: +33 5 61 33 25 93.
  E-mail addresses: stephane.perrouty@get.obs-mip.fr, perrouty@gmail.com (S. Perrouty).
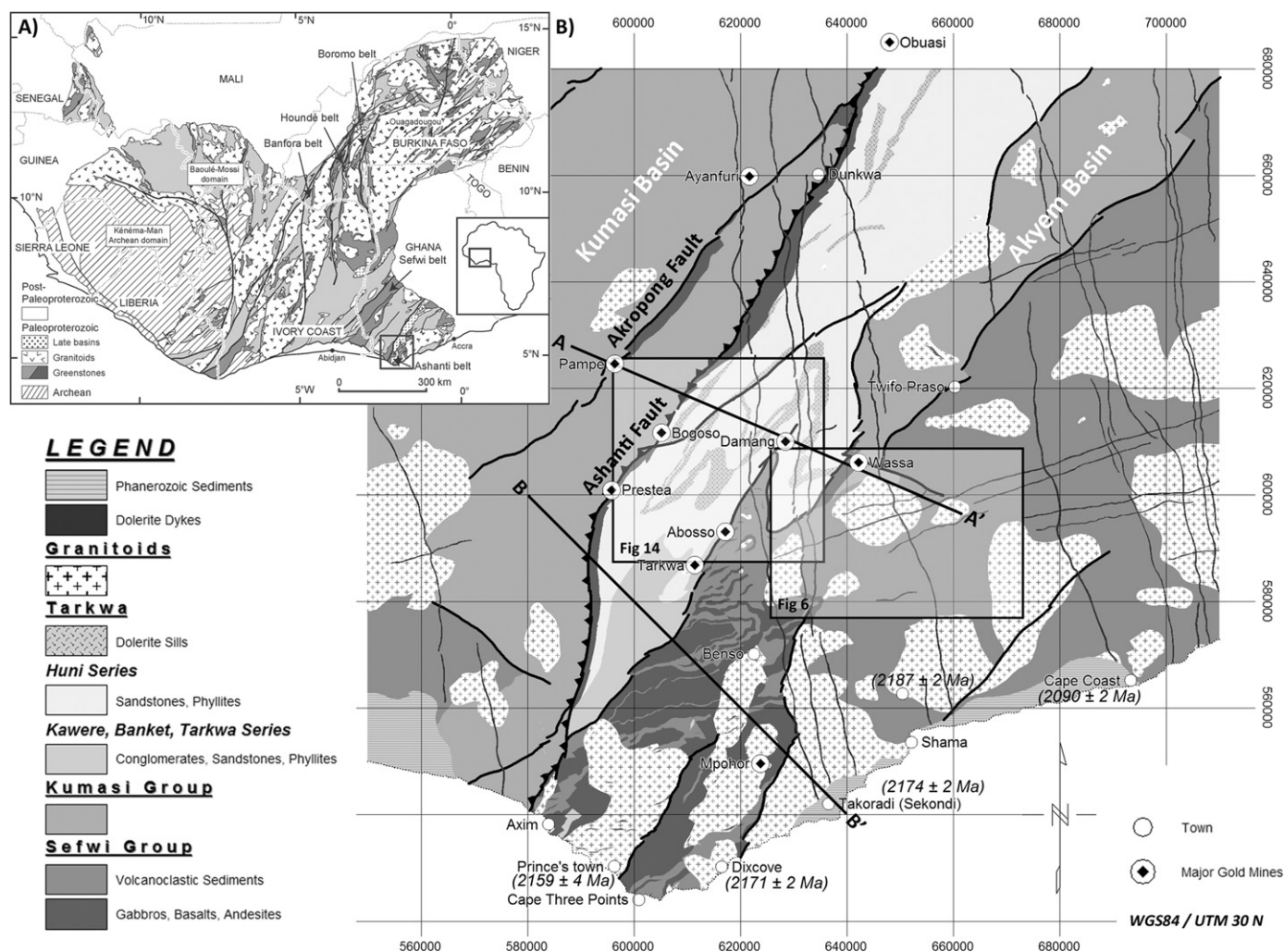
Fig. 1. (A) The West African Craton (modified after Milési et al., 2004, BRGM SIGAfrique) is composed of an Archean nucleus in the southwest bounded by series of paleoproterozoic greenstone belts and voluminous granitoids in the northwest to the east. (B) Simplified geology map of the Ashanti Belt (modified after Agyei Duodu et al., 2009) showing the locations of Figs. 6, 14 and 16.

that affected both the Birimian Supergroup and overlying Tark-waian sediments. This second phase of the Eburnean orogeny is relatively well known in the study area and is described at the mine scale (Blenkinsop et al., 1994, in Obuasi; Allibone et al., 2002a, in Obuasi and, Allibone et al., 2002b, in Bogoso; Kutu, 2003, in Konongo; Tunks et al., 2004, in Damang) and at a regional scale (Eisenlohr and Hirdes, 1992; Milési et al., 1992; Ledru et al., 1994; Barritt and Kuma, 1998; Feybesse et al., 2006).

Eburnean I events have been described along the West African Craton and called Eoeburnean in northern Ghana (De Kock et al., 2011) or Tangaean in Burkina Faso (Tshibubudze et al., 2009; Hein, 2010), but are relatively poorly resolved in southwestern Ghana. This study presents an integrated interpretation based on new field data, geophysical surveys and previous structural studies and maps (Loh et al., 1999; Agyei Duodu et al., 2009) that provides a new structural context to the Eoeburnean phase and clarifies the subsequent tectonic evolution of the Ashanti greenstone belt.

2. Geological setting

The southern part of the West African Craton, known as the Leo-Man craton, is composed of an Archean nucleus that is tectonically juxtaposed against Paleoproterozoic granitoid-greenstone assemblages to the north and east (Fig. 1). In southwest Ghana, four

NE-SW greenstone belts occur, known as the Bui, Sefwi, Ashanti and Kibi-Winneba belts from west to east, respectively. These belts are separated by three sedimentary basins namely the Sunyani, the Kumasi and the Akyem Basins (or Cape Coast Basin, Agyei Duodu et al., 2009). These greenstone belts and dividing sedimentary basins were formed and deformed during the Eburnean orogeny (Bonhomme, 1962).

2.1. Eburnean orogeny

Feybesse et al. (2006) proposed an early Eburnean phase between 2135 Ma and 2100 Ma corresponding to magmatic accretion and plutonism that terminated with development of the Kumasi Basin. The synchronous Eburnean orogeny (2130–1980 Ma) corresponds to thrust tectonism dominated by sinistral transcurrent deformation in the Ashanti Belt. Allibone et al. (2002a) suggests an alternative two phase Eburnean evolution, divided into the Eburnean I (2200–2150 Ma) and Eburnean II (2116–2088 Ma), that are separated by deposition of the Birimian and Tarkwaian units. In northern Ghana De Kock et al. (2011) called these two phases Eoeburnean and Eburnean, respectively. This nomenclature is referred to in the text, based on the correlation with published zircon geochronology (Fig. 2A).

Table 1
Comparison between the tectonic evolution presented in this work with other recent studies in southwestern Ghana.

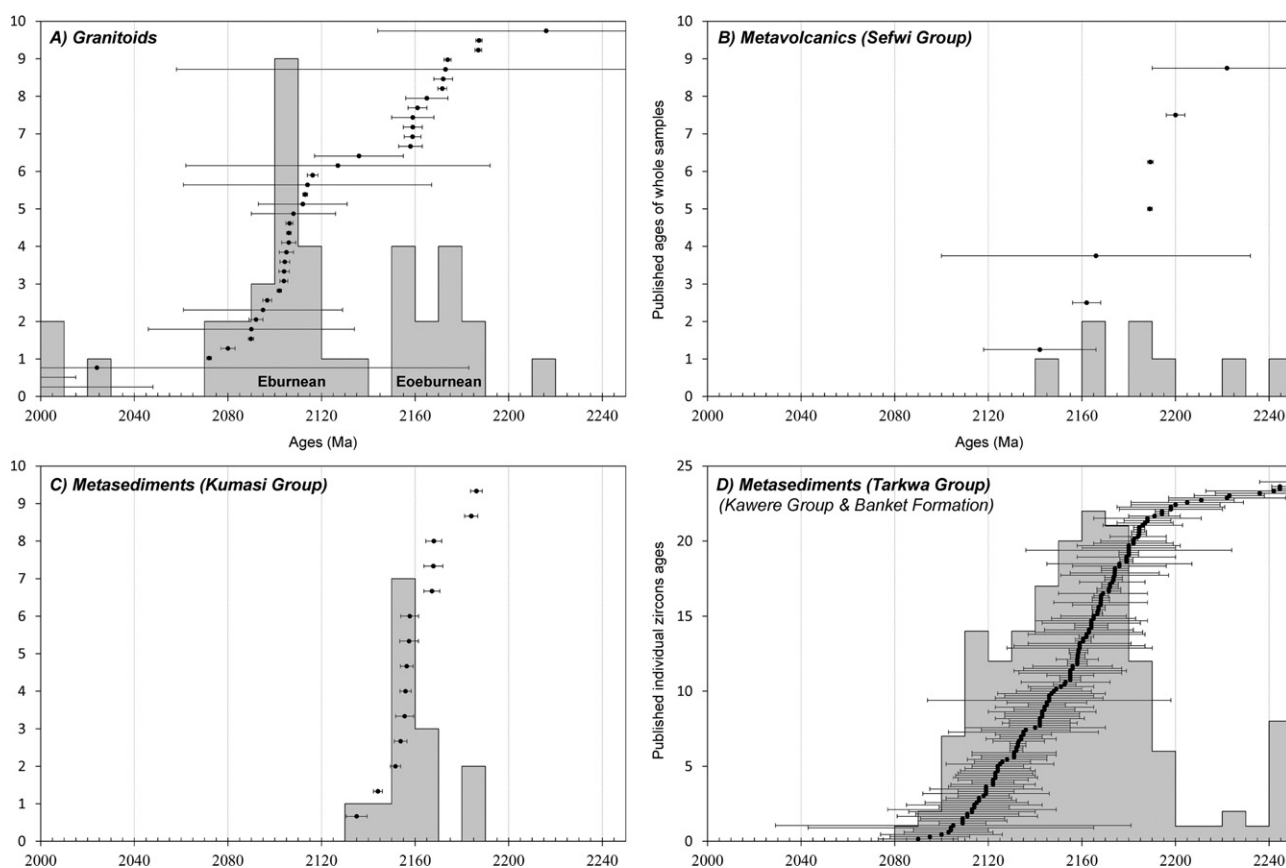|	Regional Interpretation (This Study)	In Birimian *Obuasi / Bogoso* (Allibone et al., 2002a, b)	In Tarkwaian *Damang* (Tunks et al., 2004)	Regional (Eisenlhor et al., 1992)	Regional (Feybesse et al., 2006) (Milesi et al., 1992)
Eoeburnean 2187 - 2158 Ma	Sefwi Group volcanism and sedimentation	Volcanism Granitoids intrusion Regional metamorphism		Birimian sediments and volcanics penecontemporaneous Plutonism (Dixcove type granitoids)	Magmatic accretion Plutonism Birimian sedimentation
	D1, N-S shortening Regional scale folding in the Sefwi Group Possible gold mineralization			Onset of deformation in a "foreland thrust" and Tarkwaian deposition	
	D2, Extension Phase (2154 - 2125 Ma) Kumasi Group sedimentation	D1 S1 parallel to bedding Flat-lying bedding parallel shearing			
Eburnean 2125 - 1980 Ma	**Tarkwa Basin Formation (2107 - 2097 Ma)** **D3, NW-SE shortening** Km scale folds in Birimian and Tarkwaian S3 subvertical crenulation cleavage NE-SE Thrust faults (Ashanti, Damang, …) Peak of metamorphism (2092 Ma)	D2, NW-SE shortening Isoclinal folds with axial surface parallel to the regional faults and shear zones Ashanti thrust fault	D1, NW-SE shortening Km scale folds (with subvertical surface (S1)) Damang thrust fault	D1, NW-SE shortening S1 (NE-SE) subvertical and subparallel to bedding in both Birimian and Tarkwaian Regional folds (tight to isoclinal)	D1, NW - SE shortening Thrust faults Tarkwaian sediments deposition (Syn D1) Metamorphism (6 kbar / 550 - 650 °C)
		D3 Low dip axial surface fold at Obuasi S3 crenulation cleavage overprinting S2 Final stage of D2 ?		D2, Continuing compression S2 (NE-SE) fabrics overprint S1 foliation S2 is defined by aligned muscovite and elongate recrystallised quartz grains	
	D4, NNW-SSE shortening Sinistral shear reactivation of D3 thrust S4 crenulation cleavage ENE-WSW Greenschist retrograde metamorphism Remobilization and concentration of gold particle along the shear zones and at the base of Tarkwa Basin	D4, NNW-SSE shortening Hm scale fold at Obuasi		Metamorphism	D2/D3, NW-SE shortening Tarkwaian folds Strike-slip faults and shearing Gold mineralizations Metamorphism (2 - 3 kbar / 200 - 300 °C)
		D5 or syn-D4 Sinistral strike-slip faults and shearing Gold mineralization	D2, NNW-SSE shortening Thrust faults and minor folds	Synorogenic plutonism (Cape-Coast type granitoids)	
	D5 Recumbant folds (< m) Subhorizontal crenulation cleavage Last pyrite/gold mineralization associated with quartz vein		D3, ESE-WNW shortening Folds with shallowly dipping axial surfaces and mineralized quartz veins, post-dating the peak of metamorphism	K-rich plutonism (cross-cutting all previous structures)	Late plutonism
	D6, NE-SW shortening Low amplitude folds + crenulation cleavage≈ N320 / 70 (RH) Reverse faults oriented NW-SE		D4 Faults oriented NW-SE		

Fig. 2. Compilation of histograms presenting radiometric age data and the number of zircons/whole rock samples for the three main stratigraphic sequences and on granitoids in the study area (after Taylor et al., 1992; Hirdes et al., 1992; Davis et al., 1994; Hirdes and Davis, 1998; Oberthür et al., 1998; Loh et al., 1999; Pigois et al., 2003; Attoh et al., 2006; Feybesse et al., 2006; Adadey et al., 2009; Agyei Duodu et al., 2009). The age distribution in granitoids shows two distinct peaks that correspond to the Eoeburnean and Eburnean phases. Dots represent dated samples for igneous rocks or zircons ages for sedimentary rocks and their associated error bars.

Allibone et al. (2002a) suggest that the Eburnean I (Eoeburnean) event was associated with a period of magmatism and metamorphism responsible for the Sefwi Group metavolcanics and TTG granitoid emplacement (Table 1) that correlates with the pre-Eburnean of Feybesse et al. (2006).

The second phase of the Eburnean orogeny affects both the Tarkwa Group and the Birimian Supergroup. The Eburnean II (Eburnean) event is associated with major NW-SE shortening (D2 of Allibone et al. (2002a, b); D1 of Tunks et al. (2004)) that developed major thrust faults – including the Ashanti Fault – along with isoclinal folds in Birimian metasediments and regional scale open folds in the Tarkwaian sediments. These features are overprinted by thrusts that were reactivated during a phase of sinistral transpression that utilised the existing thrust architecture (D2 of Tunks et al. (2004); D3 of Milési et al. (1992); D3 of Feybesse et al. (2006)). At the Obuasi mine, 100 m scale folds described by Allibone et al. (2002a) may have developed during (his D4–D5) shearing. This phase of the Eburnean orogeny is associated with most of the hydrothermal gold deposits in the region. Late Eburnean deformation has been observed in the Damang mine, where it is characterised by very open folding and minor brittle faulting (Tunks et al., 2004). The D3 of Tunks et al. (2004) corresponds to ESE-WNW shortening associated with folds, quartz veins and a shallow dipping crenulation cleavage that overprints D2 reactivated thrust faults. In Damang, Tunks et al. (2004) observed a conjugate system of faults that strike NW-SE and cross-cut all previous structures. These features may correlate with more regionally extensive NW-SE faults recognised in existing maps of southwestern Ghana.

The relationship and timing between Eburnean deformation and Tarkwaian deposition are contentious and not fully understood.

Allibone et al. (2002a) suggested Tarkwaian sedimentation occurred before major Eburnean deformation and mineralisation. Leube et al. (1990) played down the significance of post-Tarkwaian deformation suggesting "tension-related folding by gravity" (Stage V of Leube et al. (1990, p. 157)) was responsible for Tarkwaian structures, requiring earlier events to have controlled the regional structural architecture and the distribution of gold mineralisation. Other workers propose an intermediate position with Feybesse et al. (2006) suggesting Tarkwaian sedimentation developed in response to Eburnean shortening following a phase of tectonic accretion and magmatism. Further, Ledru et al. (1994) considered the Tarkwa Basin to have initiated as a foreland basin during the final stages of the Eburnean orogeny.

2.2. Birimian series

The Birimian series was first described by Kitson (1918) in the Birim River (around 80 km east of the Ashanti Belt). Since this early interpretation, the Birimian stratigraphic column has been revised significantly, including more than one complete reversal. Before the application of absolute geochronology, workers described an Upper Birimian composed by metavolcanics on top of a Lower Birimian corresponding to metasediments (Kitson, 1928; Whitelaw, 1929; Junner, 1935, 1940; Hastings, 1982; Ntiamoah-Agyakwa, 1979; Kesse, 1985; Milési et al., 1992). Leube et al. (1990) and Eisenlohr and Hirdes (1992) suggested that Birimian metavolcanics and metasediments were synchronous. Sm/Nd analyses conducted by Taylor et al. (1992) required a reversal of the stratigraphy with the younger metasediments overlying the older metavolcanics. This relationship was confirmed by Loh et al. (1999) with U/Pb

zircon ages varying between 2162 ± 6 Ma and 2266 ± 2 Ma for the metavolcanics. Detrital zircons in the metasediments indicate the initiation of their deposition around 2154 ± 2 Ma in the Obuasi mine (Oberthür et al., 1998). Similar ages have been found in the Kumasi Basin (northwest of the Ashanti Belt) by Davis et al. (1994). Adadey et al. (2009) proposed a new stratigraphy of the Birimian Supergroup with the Sefwi Group (2195–2170 Ma) composed of micaschists and metavolcanics and the Kumasi Group, deposited after 2150 Ma, with metasediments and intercalated andesitic beds dated at 2142 ± 24 Ma (U/Pb on zircon). The Kumasi Group was intruded by the late sedimentary Suhuma granodiorite at 2136 ± 19 Ma (U/Pb on zircon, Adadey et al., 2009).

2.3. Tarkwaian series

The Tarkwa Group (Kitson, 1928) is a succession of four sedimentary units (Whitelaw, 1929; Junner, 1940; Kesse, 1985; Pigois et al., 2003) (Table 2). The Kawere Group, at the base of the Tarkwaian sediments is composed of conglomerates and sandstones. Its thickness varies between 250 m and 700 m and is stratigraphically overlain by the Banket Formation made up of conglomerates with interbedded local cross-bedded sandstones layers. The conglomerates are principally composed of Birimian quartz pebbles (>90%) and volcanic clasts (Hirdes and Nunoo, 1994) that host the Tarkwa Placer deposit. Gold within the conglomerate forms a zone that is less than 100 m thick, while the maximum thickness of the Banket sequence is estimated to be 600 m. Approximately 400 m of Tarkwa Phyllites overly the Banket sequence. The uppermost unit of the Tarkwa Group is the Huni Sandstone, comprised of alternating beds of quartzite and phyllite intruded by minor dolerite sills that form a package up to 1300 m thick (Pigois et al., 2003).

U/Pb and Pb/Pb dating of a few detrital zircons provide a maximum depositional age of 2132 ± 2.8 Ma for the Kawere formation and 2132.6 ± 3.4 Ma for the Banket formation (Davis et al., 1994; Hirdes and Nunoo, 1994). These ages agree with the study by Pigois et al. (2003), that yielded maximum depositional age of 2133 ± 4 Ma from 71 concordant zircons from the Banket formation. However 39 of their zircons are younger and contradict this value. According to all concordant zircons histogram (161 grains) and their uncertainties (Fig. 2D), a reasonable estimation for the start of the Tarkwaian sedimentation could be as young as 2107 Ma although two zircons may be younger at 2090 ± 17 Ma and at 2095 ± 17 Ma (Pigois et al., 2003). Tarkwaian deposition is also constrained by intrusions of metagabbro sills within the Tarkwaian series at 2102 ± 13 Ma (Adadey et al., 2009) and by granitoids at 2097 ± 2 Ma (Oberthür et al., 1998).

2.4. Granitoids

Abundant granites and granitoids intruded the Birimian and Tarkwaian units during the Paleoproterozoic. Eburnean plutonism in southwest Ghana can be divided into two phases between 2180–2150 Ma (Eoeburnean) and 2130–2070 Ma (Eburnean) that is supported by the current database of U/Pb and Pb/Pb zircon ages (Fig. 2A). Most of the granitoids intruded during both phases correspond to typical tonalite–trondhjemite–granodiorite (TTG) suites. However, in the southern part of the Ashanti Belt, intrusions within the Mpohor complex have granodioritic, dioritic and gabbroic compositions. Along with this compositional heterogeneity, granitic rocks in the southern Ashanti Belt also appear to have been emplaced under different tectonic regimes. The Sekondi granodiorite on the eastern margin of the southern Ashanti Belt exhibits a magmatic foliation (Loh et al., 1999), suggesting syntectonic emplacement at around 2174 ± 2 Ma (U/Pb on zircon, Oberthür et al., 1998). In contrast, tonalites at Dixcove and Prince's Town

are unfoliated and were dated at 2171 ± 2 Ma (Hirdes et al., 1992) and 2159 ± 2 Ma (Attoh et al., 2006).

Granitoids from the Eburnean phase sometimes show a magmatic mineral alignment (biotite and/or feldspar) but are generally unfoliated. Late Eburnean granitoids are often K-feldspar rich and are mainly found in the Akyem, Kumasi and southern Sunyani basins where they cross-cut all major regional structures.

Similar ages and characteristics have been observed in granitoid intrusions in the small fragment of the Ghanaian craton in northern Brazil (the Sao Luis Craton, Klein et al., 2005, 2008). This fragment covers a small area mostly composed by granitoids. As a consequence, correlation between the Ghanain and the Sao Luis cratons can only be performed via granitoid ages and geochemistry analyses.

2.5. Dolerite dykes

Dolerite dykes are abundant across the West African craton where they cross-cut Archean and Paleoproterozoic basement. In southwestern Ghana these dykes are well defined in magnetic data where they are characterised by strong magnetic susceptibility and remanence. The recently compiled regional 1 M map of Ghana (Agyei Duodu et al., 2009) shows two families of dykes that are oriented N-S and ENE-WSW that are generally less than 100 m in thickness. In the northern Ashanti Belt these dykes are overlain by the Volta basin. Dolerite dykes are observed to cross-cut undeformed K-feldspar rich granites that formed during the late Eburnean, and are overlain by Volta basin sediments with a maximum depositional age of 950 Ma (Kalsbeek et al., 2008). These relationships constrain dyke emplacement to between 2000 Ma and 950 Ma. In contrast some older dolerite/gabbro dykes and sills were deformed during the Eburnean orogeny and are dated at 2102 ± 13 Ma (U/Pb on zircon, Adadey et al., 2009).

2.6. Phanerozoic series

The youngest lithologies in the study area correspond to Phanerozoic sandstones and shales. These can be found along the coast, mainly between Cape Coast and Takoradi but also to the west of Axim. Loh et al. (1999) distinguished two groups with ages ranging from Devonian to Carboniferous (Crow, 1952; Mensah, 1973; Chaloner et al., 1974; Baer and Riegel, 1980) and Cretaceous (Tevendale, 1950).

2.7. Metamorphism

With the exception of some late Eburnean granitoids, dolerite dykes and Phanerozoic sediments, all other lithologies have undergone metamorphism that generally does not exceed upper greenschist facies. Studies on amphibole/plagioclase assemblages suggest the peak temperature and pressure was 500–650 °C and 5–6 kbar (John et al., 1999), dated at 2092 ± 3 Ma (Oberthür et al., 1998). These results are similar to those obtained by Schmidt Mumm et al. (1997) who estimated peak metamorphic conditions along the Ashanti Fault system to 520 °C and 5.4 kbar. These conditions are in agreement with the occurrence of garnet in the Nsuta manganese deposit (Nyame et al., 1998; Kleinschrot et al., 1993, 1994) and garnet-staurolite assemblages at the Damang gold mine (Pigois et al., 2003), although these manganese-rich garnet assemblages can be stable to lower pressure and temperature conditions (Mahar et al., 1997). Occurrences of kyanite and sillimanite assemblages have also been reported from the Bonsa diamond field (Kesse, 1985).

Table 2
Division of Tarkwaian sedimentary sequences and estimated thicknesses.

Tarkwaian unit		Thickness Whitelaw (1929)	Junner (1940)	Kesse (1985)	Pigois et al. (2003)
Huni sand- stones	Dompin quartzites	1000 ft (300 m)	4500 ft	1370 m	>1300 m
	Dompin phyllites	500 ft (150 m)	(1370 m)		
	Huni sandstones	1500 ft (450 m)			
Dolerite sills			600 ft (180 m)		<200 m
Tarkwa phyllites		800–1000 ft (240–300 m)	600 ft (180 m)	120–400 m	120–400 m
Banket Group	Sandstones	2100 ft (640 m)	500–600 ft (150–180 m)	100–180 m	150–600 m
	Mineralised conglomerates		100–300 ft (30–90 m)	20–90 m	
	Sandstones		1000 ft (300 m)	150–350 m	
Kawere Group	Conglomerates levels interbedded with sandstones and phyllites			250–700 m	250–700 m

2.8. Mineralisation

The Ashanti Belt of southwest Ghana hosts a gold district that contains a significant number of world class hydrothermal gold deposits and the giant Obuasi deposit that hosts over 60 million ounces of gold. These deposits are spatially associated with the Ashanti Fault and other major shear zones in the Birimian Super-group or along the contact between the Birimian and Tarkwaian units. The overlying Tarkwa Basin is also host to the Tarkwa paleo-placer that contains over 40 million ounces of gold.

2.8.1. Birimian deposits

Deposits found along the Ashanti Fault are associated with arsenopyrite and lesser other sulphides. According to Oberthür et al. (1994, 1997) and Allibone et al. (2002a) the main mineral-isation in the Obuasi mine is associated with ductile shearing along the Ashanti Fault. They also described secondary gold mineralisa-tion that developed within quartz veins and carbonate-alteration in basalts. In the Bogoso and Prestea deposits, Mumin et al. (1994) showed that gold mineralisation resulted from the remobilisation of pre-existing gold along the Ashanti Fault. The source of initial gold mineralisation has not been clearly identified.

Birimian mineralisations are often hosted within shear zones that transect sediments, mafics or granitoids (Table 3, after Bowell et al., 1990; Schwartz et al., 1992; Klemd et al., 1993; Mumin and Fleet, 1995; Mumin et al., 1996; Schmidt Mumm et al., 1997; Yao and Robb, 2000; Yao et al., 2001; Allibone et al., 2002a, b; Griffis et al., 2002; Pigois et al., 2003; Tunks et al., 2004; Wille and Klemd, 2004). Fluid inclusions studies propose low temperature ($\approx$250 °C) and pressure ($\approx$2 kbar) homogenisation conditions for fluid trapped in mineralised Birimian quartz veins and pebbles (Schmidt Mumm et al., 1997).

Few radiometric ages have been acquired from the Birimian deposits. Near Ayanfuri, mineralisation is associated with gran-itoids dated at 2105 ± 3 Ma for the intrusion (U/Pb on zircon, Oberthür et al., 1998) and 2084 ± 2 Ma (Pb/Pb) for rutile/galena crystallisation from hydrothermal fluids (Oberthür et al., 1998).

2.8.2. Tarkwaian deposits

Two styles of gold mineralisation are present in the Tarkwa Group. Hydrothermal deposits occur along the contact between the Birimian and Tarkwaian units (e.g. Damang Mine), and paleoplac-ers occur within the Tarkwa Basin (e.g. Tarkwa Mine). In Damang, gold mineralisation was found to be associated with pyrite in brit-tle fractures and tensional quartz veins that are correlated with the last deformation phase of the Eburnean orogeny (Tunks et al., 2004). The late timing of mineralised structures was supported by a xeno-time age of 2063 ± 9 Ma (U/Pb, Pigois et al., 2003). Fluid inclusions

within quartz veins associated with mineralisation formed at low temperature (153–278 °C) and pressure (1–2.2 kbar) homogenisa-tion conditions in the Abosso-Damang deposits (Schmidt Mumm et al., 1997).

Tarkwaian sediments also host paleoplacers such as the Tarkwa deposit. Gold grade distribution within the deposit is parallel to bedding, supporting a sedimentary origin (Sestini, 1973). Gold is generally found within paleochannels, along conglomerates and proximal to hematite rich areas within the Banket formation (Table 2). Fluid inclusions studies of mineralised quartz pebbles suggest formation under greenschist facies conditions (250–400 °C and 0.5–3 kbar, Klemd et al., 1993). These values are similar to those obtained for Kumasi Group quartz veins fluid inclusions along the Ashanti Belt, and may explain why the source of the Tarkwa placer has been initially described as a Birimian type hydrothermal deposit (Klemd et al., 1993; Hünken et al., 1994).

3. Data used for mapping

3.1. Field data

In order to ground truth and constrain the geophysical interpre-tation, petrophysical, structural and lithological data were collected across the southern Ashanti Belt. These data were then combined with pre-existing observations and outcrop maps from Loh et al. (1999) and company data from explorers within Ghana (BHP and Golden Star).

Despite collecting data from most of the accessible outcrops in the study area, the presence of a thick lateritic blanket restricts the use of traditional mapping and only allowed for the sparse collec-tion of geological data. In general, the weathered cover sequence presents as 6–15 m of laterite underlain by 40 m of saprolite.

In order to complement the previous regional mapping, geo-physical data were used to extrapolate the structures between the isolated outcrop observations and petrophysical data were used to constrain the geophysical modelling.

3.2. Processing and interpretation of geophysical data

Magnetic and radiometric data were acquired between 1994 and 1996 by the Geological Survey of Ghana. The flight altitude of the survey is 80 m above ground, along lines striking 135° and separated by 200 m. The total magnetic intensity (TMI) was gridded with a resolution of 100 m.

3.2.1. Aeromagnetic data

The data were reduced to the pole ($D = -6.5°$, $I = -14.5°$) (RTP, Fig. 3) in order to bring anomalies directly over their causative

Table 3
Synthesis of structural and fluid inclusion studies for major gold deposits of southwestern Ghana. P–T data correspond to the homogenisation temperature and pressure of aqueous-carbonic inclusions in quartz veins and pebbles.

|	Gold Deposits	Host Rock	Structural Context	Pressure	Temperature	P-T Reference
Birimian	*Obuasi*	Phyllites, Volcanoclastics, Basalts	Shear zones related fractures	-	267 / 340 °C [1]	Bowell et al., 1990
	(60 Moz)	(Kumasi / Sefwi / Tarkwa groups contacts)	(Ashanti and Akropong faults)	> 0.8 kbar	165 / 220 °C [2]	Bowell et al., 1990
			Late D3 to Syn-D4	> 0.8 kbar	145 / 175 °C [3]	Bowell et al., 1990
				1 - 2.2 kbar	215 / 405 °C	Schwartz et al., 1992
		Eburnean Granodiorites - Tonalites	Sheared plutons margins	1 - 3 kbar	180 - 350 °C	Yao et al., 2000
			Late D3 to Syn-D4			
	Bogoso	Phyllites, Basalts	Graphitic shear zone (Ashanti Fault)	1 - 2 kbar	140 - 340 °C	Mumin et al., 1995, 1996
	(4 Moz)	(Sefwi Group / Kumasi Group contact)	Late D3 to Syn-D4			
	Prestea	Phyllites, Basalts	Graphitic shear zone (Ashanti Fault)	1 - 2 kbar	220 - 390 °C	Mumin et al., 1995, 1996
	(11 Moz)	(Kumasi / Sefwi / Tarkwa groups contacts)	Late D3 to Syn-D4	2 - 4 kbar	290 - 323 °C	SchmidtMumm et al., 1997
	Ayanfuri	Eburnean Tonalites	Shear zone (Akropong Fault)	1 - 2.2 kbar	278 - 334 °C	SchmidtMumm et al., 1997
	(1 Moz)		Late D3 to Syn-D4	0.7 - 2.9 kbar	220 - 280 °C	Wille et al., 2004
				0.9 - 3 kbar	209 - 330 °C	Yao et al., 2001
	Mpohor	Eoeburnean ? Gabbros, Granodiorites	Late shear zone and felsic dyke intrusion	1.1 - 3 kbar	197 - 320 °C	Yao et al., 2001
	(2 Moz)		D5 ? or D6 ?			
Tarkwaian	*Abosso - Damang*	Sandstones, Phyllites, Dolerites	Late Eburnean quartz veins, fault-related	1 - 2.2 kbar	153 - 278 °C	SchmidtMumm et al., 1997
	(8 Moz)	(Sefwi Group / Tarkwa Group contact)	D5 ?, 2063 ± 9 Ma (U/Pb on hydrothermal xenotime, Pigois et al., 2003)			
	Tarkwa	Banket Conglomerates	Tarkwa Group sedimentation	0.5 - 3 kbar	250 - 400 °C	Klemd et al., 1993
	(41 Moz)	(Placer deposit)	Early D3			
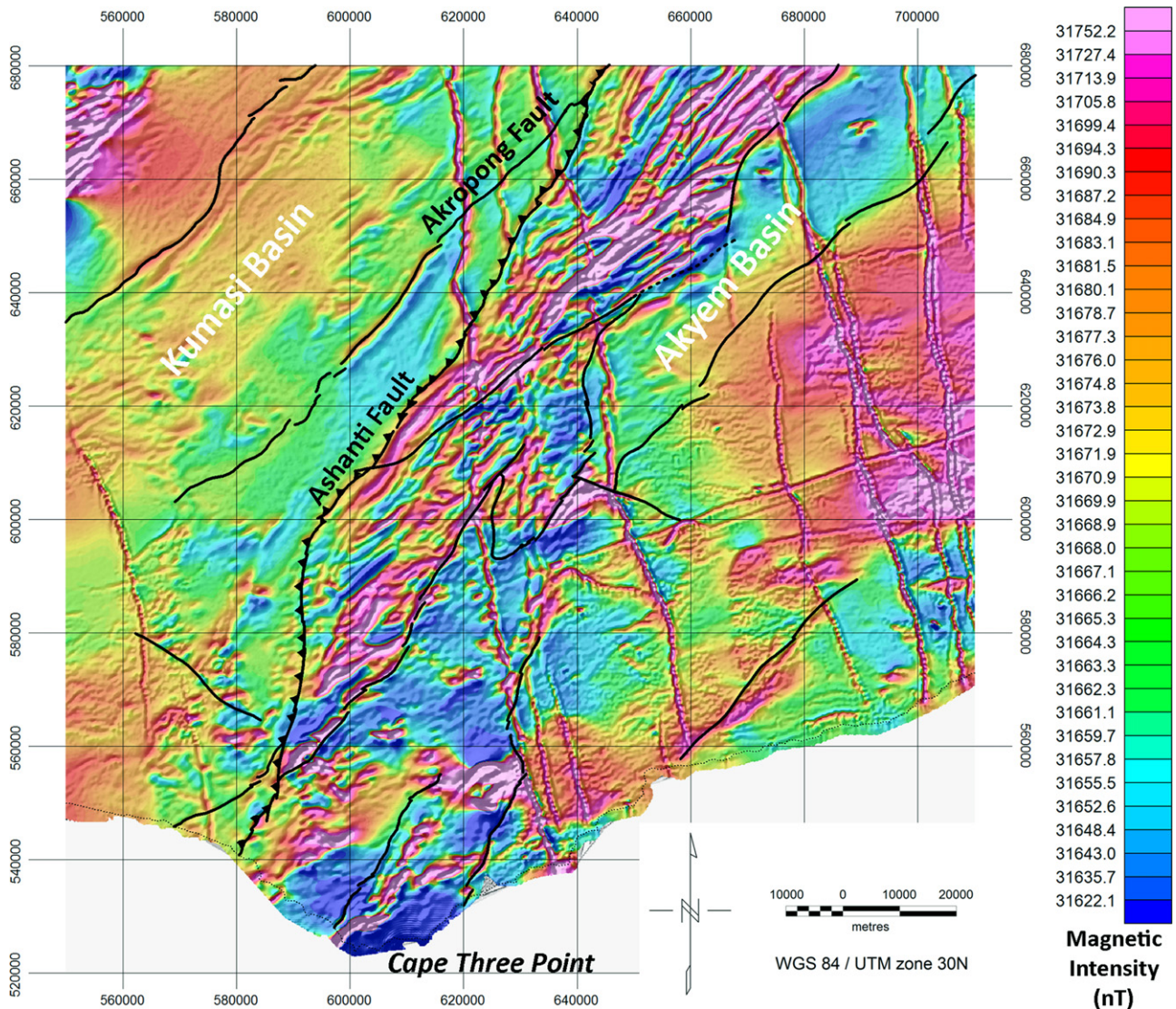
Fig. 3. The reduced to pole image of the total magnetic intensity draped over the shaded first vertical derivative. This image was the basis for all subsequent processing and is shown in respect with some of the main Ashanti and other significant regional faults. Pixel size is 100 m. The colour look up table is histogram equalised.

sources. The reduction to the pole was applied without amplitude correction (minor N-S artefacts appears) or with amplitude correction (no artefacts and similar resulting image but different magnetic intensity values). The RTP with amplitude correction was used preferentially for visual interpretation of structures as the absolute values of anomalies are less important than their geometry. Both the RTP and the analytic signal grids (which produce similar images as the RTP, MacLeod et al., 1993) were then filtered to produce further interpretable images that highlighted specific elements of the geology. The first and second vertical derivative and amplitude normalisation (Automatic Gain Control, AGC) and the tilt derivative (Verduzco et al., 2004; Lahti and Karinen, 2010) were also used to highlight structural information (Gunn et al., 1997; Milligan and Gunn, 1997), and upward continuation was applied to highlight the 'deeper' magnetic anomalies.

3.2.2. Radiometric (gamma-ray) data

U, Th and K bands have been gridded separately at 100 m resolution. These bands were then combined in a ternary RGB image and draped over a digital elevation model (90 m resolution; Shuttle Radar Topographic Mission, 2000) (Fig. 4). The combination of

radiometric data and the digital elevation model helped delineate lithological domains and structures (Dickson and Scott, 1997).

Due to the relatively subdued topography in the study area (between sea level and 460 m), the variation in elevation corresponds to differential erosion of resistant lithologies. For example, topographic relief along the Ashanti and Akropong faults and near Cape Three Points corresponds to rich Th and U areas. Similar mapping in Burkina Faso (Metelka et al., 2011) shows that these Th and U rich areas correlate with regolith cover. In contrast in SW Ghana these areas correspond to mafic rocks with strong magnetic signatures that are imaged in the aeromagnetic data and confirmed on the field. Using the methodology of Metelka et al. (2011), we help to identify some lithological units and structures by comparison between magnetic, radiometric and topography data (Table 4).

3.2.3. Gravity data

Gravity data have been sourced from the International Gravimetric Bureau (http://bgi.omp.obs-mip.fr/) as Free Air and Bouguer anomalies grids. Fig. 5 shows the Bouguer anomaly map calculated using density values of 2.67 g/cm^3 for the Bouguer correction that were gridded at 2.5 arc-minute (approximately 4.6 km). These

Table 4

Summary table of the lithologies, associated petrophysics properties and geophysical signatures (modified after Metelka et al., 2011). The magnetic image is composed of the RTP draped over the shaded first vertical derivative. The radiometric image is draped over the shaded digital elevation model. Whole rock geochemical analyses were conducted by A.L.S. Mineral Laboratory, Sevilla, Spain. (For interpretation of the references to colour in this Table, the reader is referred to the web version of this article.)
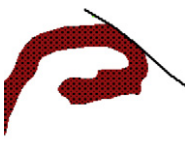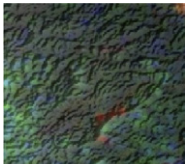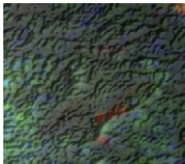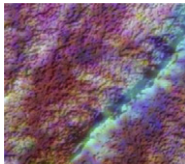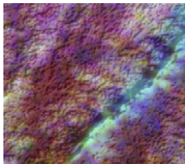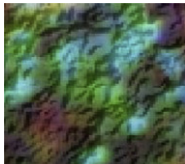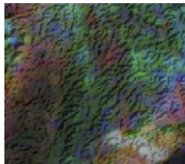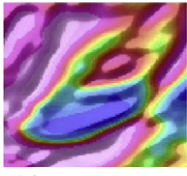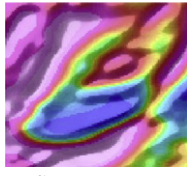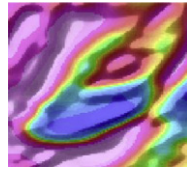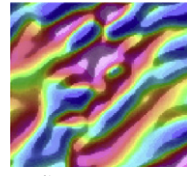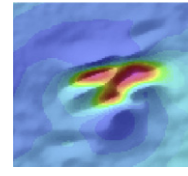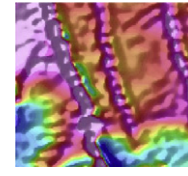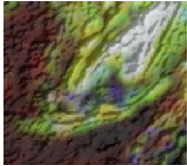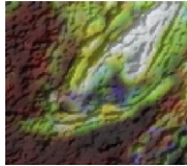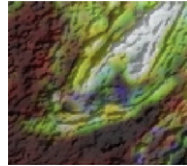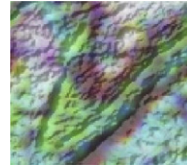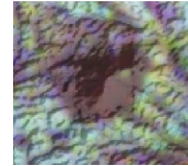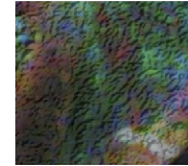
	Birimian					Late Dykes
Lithology	Micaschists	Volcanoclastic metasediments	Phyllites	Metabasalts Metaandesites	Metagabbros	Dolerite (dykes)
Mineralogy	qz, pl, chl, ms, bt, gph, gt	qz, pl, chl, bt	chl, ms, bt, gph, qz, ep	chl, bt, pl, qz, ser, ank, dol, cal	cpx, hbl, pl, chl, bt, qz	ol, opx, cpx, hbl, bt, pl
Susceptibility range (10^{-3} SI)	0.24–0.32	0.24–0.56	0.06–0.60	0.09–4.22	0.35–24.70	25.13–30.90 (+remanence)
Sample	GH101B	GH504	GH515	GH503	GH129G	GH370
U (ppm)	1.440	0.460	0.460	0.350	0.310	0.800
Th (ppm)	5.100	1.650	1.030	1.220	0.750	3.120
K_2O (%)	3.150	1.360	1.120	1.130	0.610	1.030
Map	8 km	8 km	8 km	8 km	8 km	8 km
Airborne magnetic response	Moderate intensity domains. Strong magnetic fabric (parallel to bt. alignment)	Moderate intensity layers	Low intensity domains, uniform	Moderate to high intensity layers	High intensity bodies	High intensity linear features
Airborne radiometric response	Medium U, High Th, Medium K (dark green)	Low U, Medium Th, Low K (green)	Low U, Low Th, Medium to high K (red-violet)	Low U, Th, K. Often covered by high U, Th regolith (blue-green)	Low U, Th, K. Often covered by high U, Th regolith (blue-green)	Low U, High Th, Low K (green)

Table 4 (*continued*)

	Tarkwaian			Eburnean intrusions		Eoeburnean intrusions
Lithology	Phyllites	Sandstones	Conglomerates	Dolerite (sills)	Granite Granodiorite	Granodiorite Tonalite
Mineralogy	chl, ms, bt, gph, st, gt	qz, mgt, bt	qz, Birimian and Granitoid pebbles	cpx, hbl, pl, chl, bt, gt, cal	bt, ms, qz, pl, kfs	pl, qz, bt, chl, ep
Susceptibility range (10^{-3} SI)	0.08–0.16	0.08–0.32	0.13–13.10	No data	0.06–38.00	0.05–8.06
Sample	GH397	GH512	No Sample	GH395	GH237	GH507
U (ppm)	4.500	0.880	No data	0.740	0.650	0.110
Th (ppm)	9.290	3.580	No data	2.220	1.510	0.270
K_2O (%)	2.640	1.050	No data	0.140	2.120	0.170
Map	8 km	8 km	8 km	8 km	8 km	8 km
Airborne magnetic response	Moderate intensity layers	Low intensity layers	Moderate to high intensity layers	Moderate to low intensity layers	Moderate to high intensity bodies	Low intensity bodies Strong magnetic fabric (parallel to bt. alignment)
Airborne radiometric response	High U High Th Medium K (white-yellow)	Medium U High Th Medium K (green-yellow)	Low U Low Th Medium K (dark red)	Medium U High Th Low K (light green)	Low U Low to medium Th Medium K (dark red)	Low U Low to medium Th Low K (dark red-green)

ank, ankerite; bt, biotite; cal, calcite; chl, chlorite; cpx, clinopyroxène; dol, dolomite; ep, epidote; gph, graphite; gt, garnet; hbl, hornblende; mgt, magnetite; ms, muscovite; ol, olivine; opx, orthopyroxene; pl, plagioclase; qz, quartz; ser, sericite; st, staurolite.
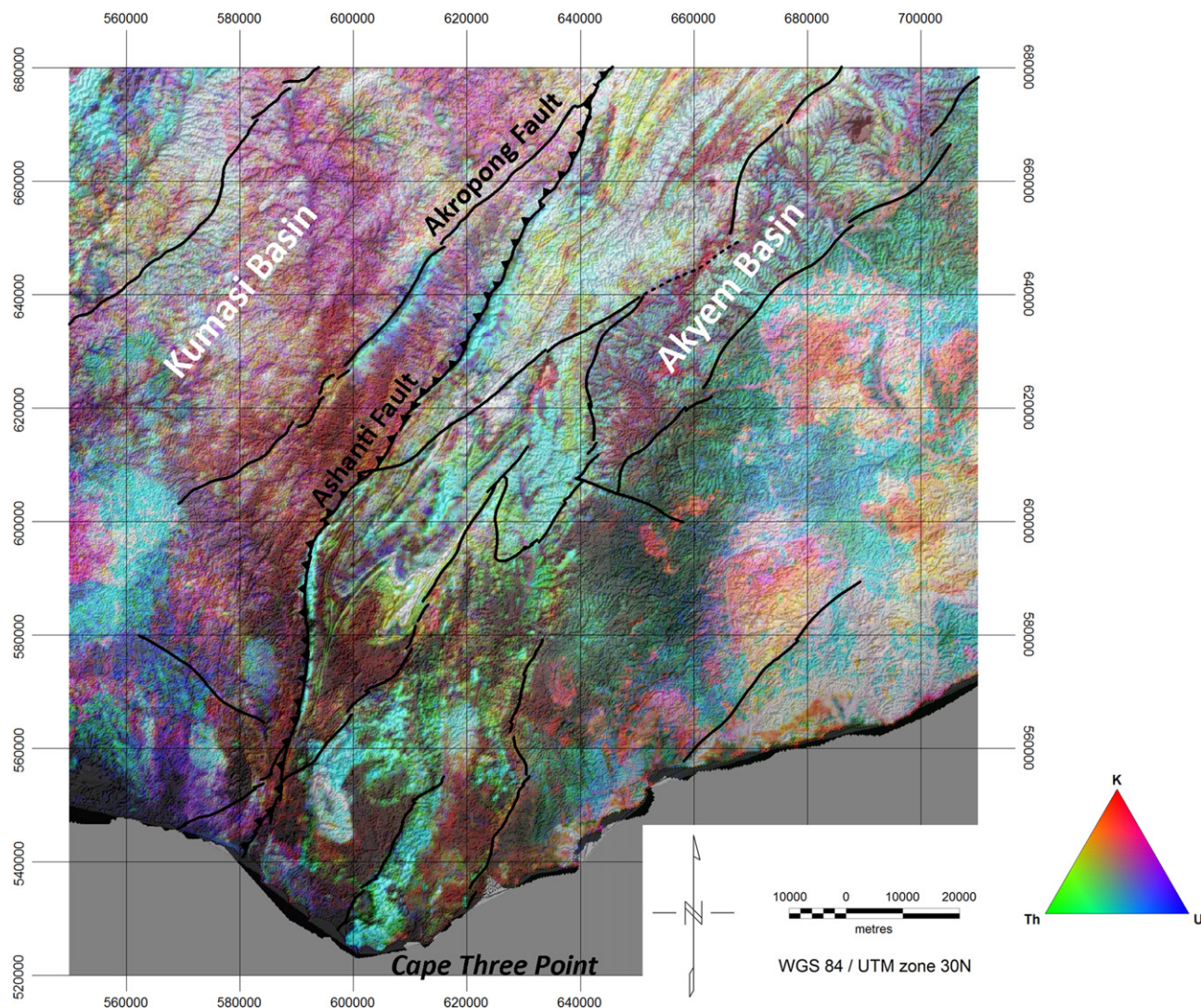
Fig. 4. Image of the gamma-ray data draped over a shaded digital elevation model. This image shows the relative proportion of potassium, thorium and uranium as an RGB image, and their correlation with the topography. Pixel size is 100 m. U and Th rich areas with high topography correspond to Sefwi Group metavolcanics as around Cape Three Points and proximal to the Ashanti Fault. K-rich granitoids are well defined in the eastern part of the area.

gravity data can only be used to broadly differentiate regional rock packages and image the continuity of the major structures at depth.

3.2.4. ALOS PALSAR data

Advanced Land Observing Satellite; Phased Array type L-band Synthetic Aperture Radar high-resolution data (ALOS PALSAR data) collected in 2009 were used to image structure within lithological packages. Two polarisation channels (HH and HV) (available from http://www.eorc.jaxa.jp/ALOS/en/) were gridded with a resolution of 50 m. A ternary RGB image was then produced (Fig. 6), where red, green, blue colours correspond respectively to the HH, HV and (HH + HV/2) polarisations. These radar data are able to image structural details within sedimentary units such as bedding, with better resolution than the combined radiometric and digital elevation model.

3.3. Petrophysics

Petrophysical data were collected during regional reconnaissance, resulting in a database of over 300 susceptibility measurements of the major lithologies encountered in the Ashanti region. The data provided quantitative information on the magnetic

susceptibility of the Birimian and Tarkwaian units and intrusives that were used to constrain the regional magnetic interpretation and subsequent geophysical modelling. These susceptibility data are consistent with common susceptibility range proposed by Clark (1997) and with values measured by Metelka et al. (2011) in Burkina Faso.

The histograms in Fig. 7 show the range of measured magnetic susceptibilities for the lithologies seen in the study area using a Geofyzika KT-5 Kappameter hand held susceptibility meter. To ensure high quality measurements, some representative samples were re-measured using a Kappabridge KLY-3 magnetic susceptibility meter and no statistically significant differences were found. Natural remanent magnetisation (NRM) of the dolerite dykes was measured using AGICO JR5A spinner magnetometer, mounted within Helmholtz coil systems. Paleomagnetic laboratory experiments were carried out at the GET Magnetism Laboratory (Toulouse).

Density data were acquired for 26 samples taken from all of the outcropping regional units. Calculated values derived from sample weighing in air and water (Table 5) agree with measurements made by Hasting (1978, unpublished report referenced in Barritt and Kuma (1998) and with equivalent samples from Burkina Faso (Baratoux et al., 2011).
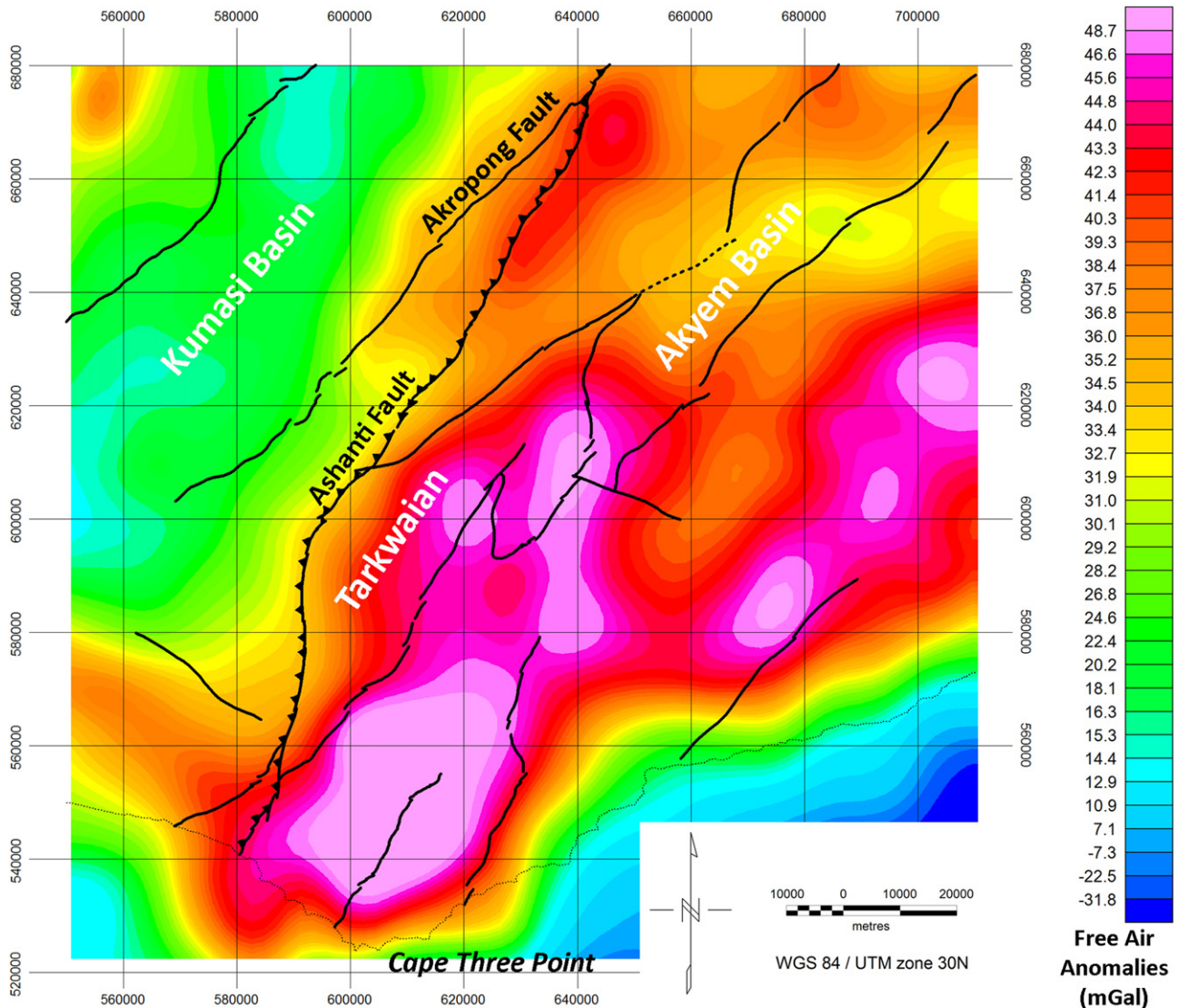
Fig. 5. Bouguer gravity map over the study area overlain with the regional fault architecture. As a consequence of the low resolution of the grid (5 km per pixels), only long wavelength features are observed, these features are interpreted to be sourced from the major, deep-seated structures.

4. Results

4.1. Birimian stratigraphy

Based on the lithologies encountered in the field, the stratigraphy of the Birimian Supergroup has been redefined in agreement with Adadey et al. (2009) nomenclature. Although individual units could be further subdivided into many thin individual layers, for clarity we have grouped these into the relatively schematic stratigraphy presented in Fig. 8.

The Sefwi Group is composed of alternating micaschists, metavolcanics and intrusive rocks (Fig. 8). Micaschists are mainly composed of quartz–muscovite–biotite, rare garnet that dominante the southeast of the Ashanti Belt (Fig. 1). Metavolcanics consist of basalts (sometimes pillow-lavas, as near Butre village, east of Cape Three Point, Fig. 1), andesites, gabbros and diorites that are found in the south of the Ashanti Belt proximal to major faults or shear zones. These metavolcanics are locally altered by quartz–sericite–carbonate hydrothermal alteration.

The Kumasi Group contains to metasediments: volcanoclastics and phyllites that are locally rich in graphite. This group is found in two major areas corresponding to the Kumasi Basin and to the Akyem Basin (Fig. 1).

4.2. Structural evolution of the Ashanti Belt

We have been able to distinguish six discrete deformation events which affected the Ashanti Belt during the Paleoproterozoic Eburnean orogeny. These six events are defined on the basis of detailed structural analysis at the outcrop scale, and geophysical interpretation at the regional scale. These methods allow the correlation of structure across the study area, and can image overprinting relationships between successive deformation events.

The Sefwi Group represents a "basement" composed by a series of basalts and volcanoclastic sediments intruded by gabbros. To the west of the Benso gold mine, a volcanoclastic unit in the Sefwi Group displays syn-sedimentary normal faulting (Fig. 9). Two thrust faults observed at this locality (Fig. 9) may reflect reactivation of these syn-sedimentary normal faults during the early Eoeburnean phase.
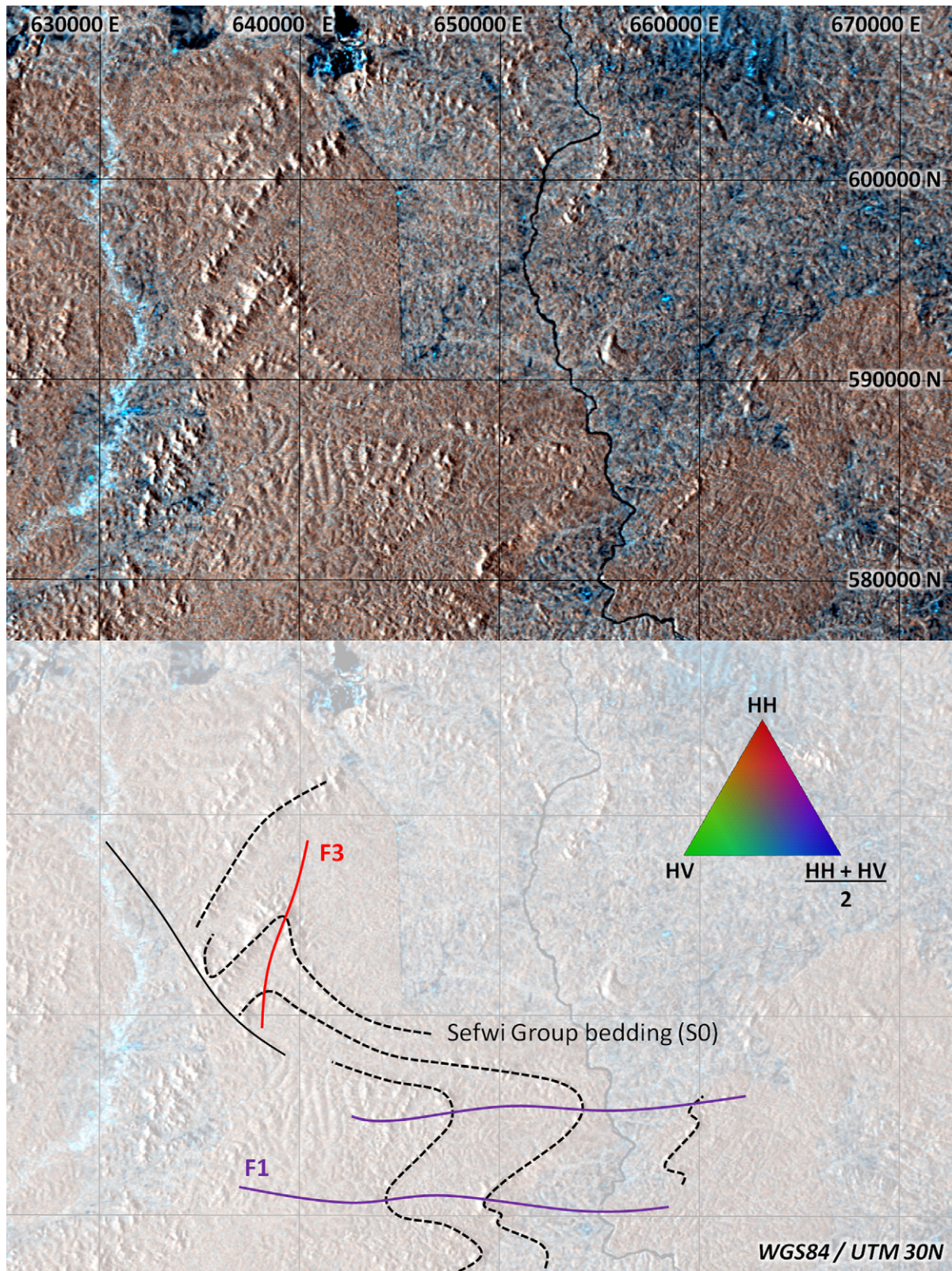
Fig. 6. ALOS PALSAR radar image consisting of three colour bands: red, HH radar polarisation; blue, HV; and green, the mean of both bands. Sefwi Group bedding highlighted by volcanoclastic layers in this image is folded by E-W trending F1 folds that are refolded by N-S trending F3 folds. See Fig. 1 for location. (For interpretation of the references to colour in this figure legend, the reader is referred to the web version of this article.)
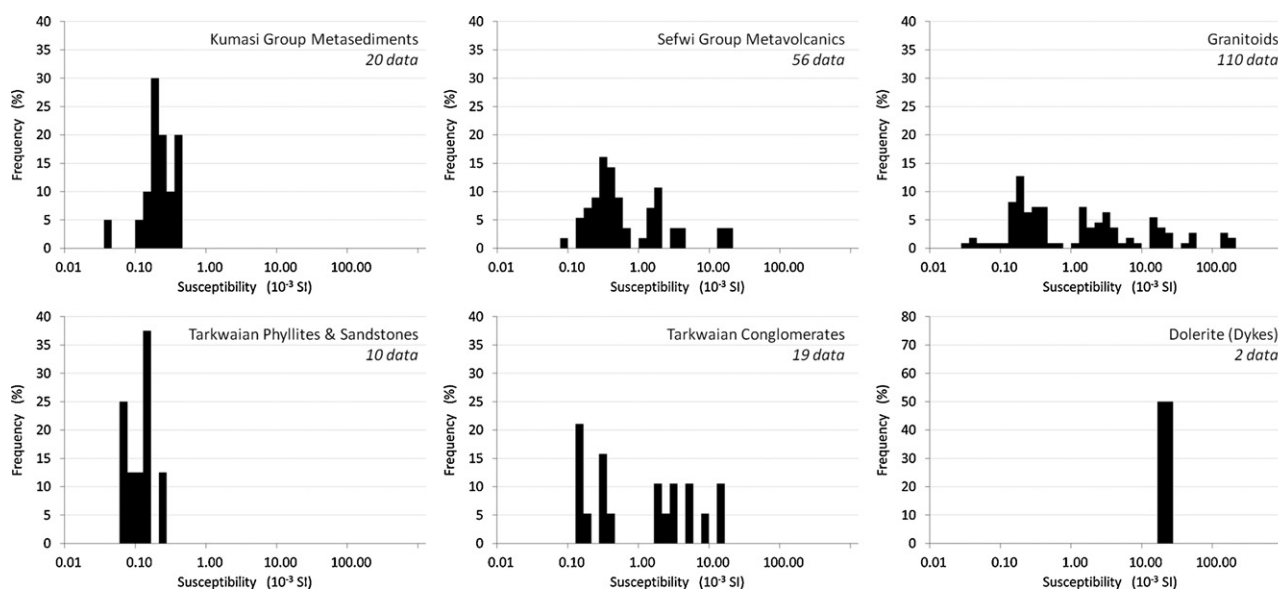
Fig. 7. Histograms showing the range of measured susceptibility for each rock type found in the area. Several samples were remeasured under laboratory condition to confirm the field based data. The susceptibility of sediments is commonly ten times lower than volcanic rocks. Granitoid susceptibilities are variable with the highest values obtained from dioritic composition. Late doleritic dykes display high magnetic susceptibility values.

4.2.1. D1 (Eoeburnean)

Our D1 corresponds to N-S shortening that produced kilometric scale folds within the Sefwi Group. Near Shama village in the SE of the Ashanti Belt, rare field evidence of D1 deformation exists as highly deformed micaschists that alternate with basaltic layers. The relatively competent basalts are strongly boudinaged and define a bedding parallel S1 foliation. In other regions, S1 is oriented approximately E-W (Fig. 10A) and is defined by the alignment of biotite (Fig. 11A). Large-scale F1 folds are imaged using high-resolution radar revealing major F1 folds within volcanoclastic units (S0) of the Sefwi Group that are refolded by F3 folds (Fig. 6).

Two discrete generations of quartz veins and pegmatite intrusions are distinguished. Early veins and intrusions are sub-parallel to bedding and often strongly boudinaged. According to their extension direction (subvertical at the time of formation for veins parallel to bedding), they should have formed pre or syn-D1. Second generation veins and pegmatites cross-cut this composite S0–S1 fabric and were developed during D1. Both generations are refolded during subsequent D3 shortening.

D1 deforms only the Sefwi Group basement, and is not observed in the overlying Kumasi and Tarkwa groups. This relationship suggests that these younger sedimentary packages were deposited after D1 and before subsequent deformation events (D3–D6).

4.2.2. D2

D2 corresponds to an extensional phase associated with the opening of the Kumasi and Akyem basins into which the Kumasi Group was deposited (Fig. 1). On the western side of the Ashanti Belt at the Prestea and Bogoso mines, the west-dipping Ashanti Fault marks the contact between Sefwi Group basement and Kumasi Group sediments. The early history of this fault contact is obscured by significant thrust and shear reactivation during D3 and D4.

On the eastern side of the belt, in Damang, the Sefwi/Tarkwa Group contact has been faulted and sheared during later deformation. This sheared contact is represented by a 2 cm thick anastomosed fabric that was probably created during D3/D4 shear reactivation of an original sedimentary contact (erosion surface), or by reactivation of an existing faulted contact that was controlling the development of the Tarkwa Basin in the eastern Ashanti Belt. As a consequence of a strong overprinting of the original sedimentary contacts during Eburnean deformation, the tectonic context of the Tarkwa Group deposition remains unclear.

4.2.3. D3 (Eburnean)

D3 deformation is conspicuous within both the Birimian and Tarkwaian units in the study area. NW-SE shortening produced km scale folds and a strong sub vertical crenulation cleavage within the Birimian and Tarkwaian units (striking around N040; Fig. 10A). Stereonets of bedding from the Kumasi Group and Tarkwa Group define a single major folding event associated with NW-SE shortening. However, the orientation of bedding within the Sefwi Group reflects the interference between D1 and D3 folds (Fig. 10A). The overprinting between F1 and F3 fold occurs across the region at multiple scales. In the Sefwi Group near Shama village, a composite S0–S1 foliation is crenulated and partially transposed along the S3 cleavage (Fig. 11A). Ptygmatic F3 folds are also found where they

Table 5
Ranges of density values measured on 26 samples of the main lithologies in Ghana (this study) and in Burkina Faso (Baratoux et al., 2011).

Unit	Density ranges (g/cm³)		
	This study	Baratoux et al. (2011)	Hasting (1978)[a]
Dolerite (Sill and Dykes)	2.87–2.90	2.92–2.93	
Mpohor Mafic Complex (Gabbro, Diorite)	2.65–3.03		
Eburnean granitoids	2.58–2.75	2.60–3.25	2.41–2.76
Eoeburnean granitoids	2.76–2.89		
Tarkwa Group (Conglomerates, Quartzites, Phyllites)	2.68–2.99	2.71–2.77	2.45–2.84
Kumasi Group (Birimian Phyllites)	2.69		2.71–2.74
Sefwi Group (Birimian) Cape Coast Mica Schists	2.65		
Volcanoclastics	2.70–2.84	2.66–2.99	2.74–3.00
Basalts/Andesites	2.84–2.93	2.72–2.97	
Gabbros	3.01	3.07–3.11	

[a] Density ranges after Hasting (1978, unpublished report referenced in Barritt and Kuma (1998)).

Stratigraphic Column
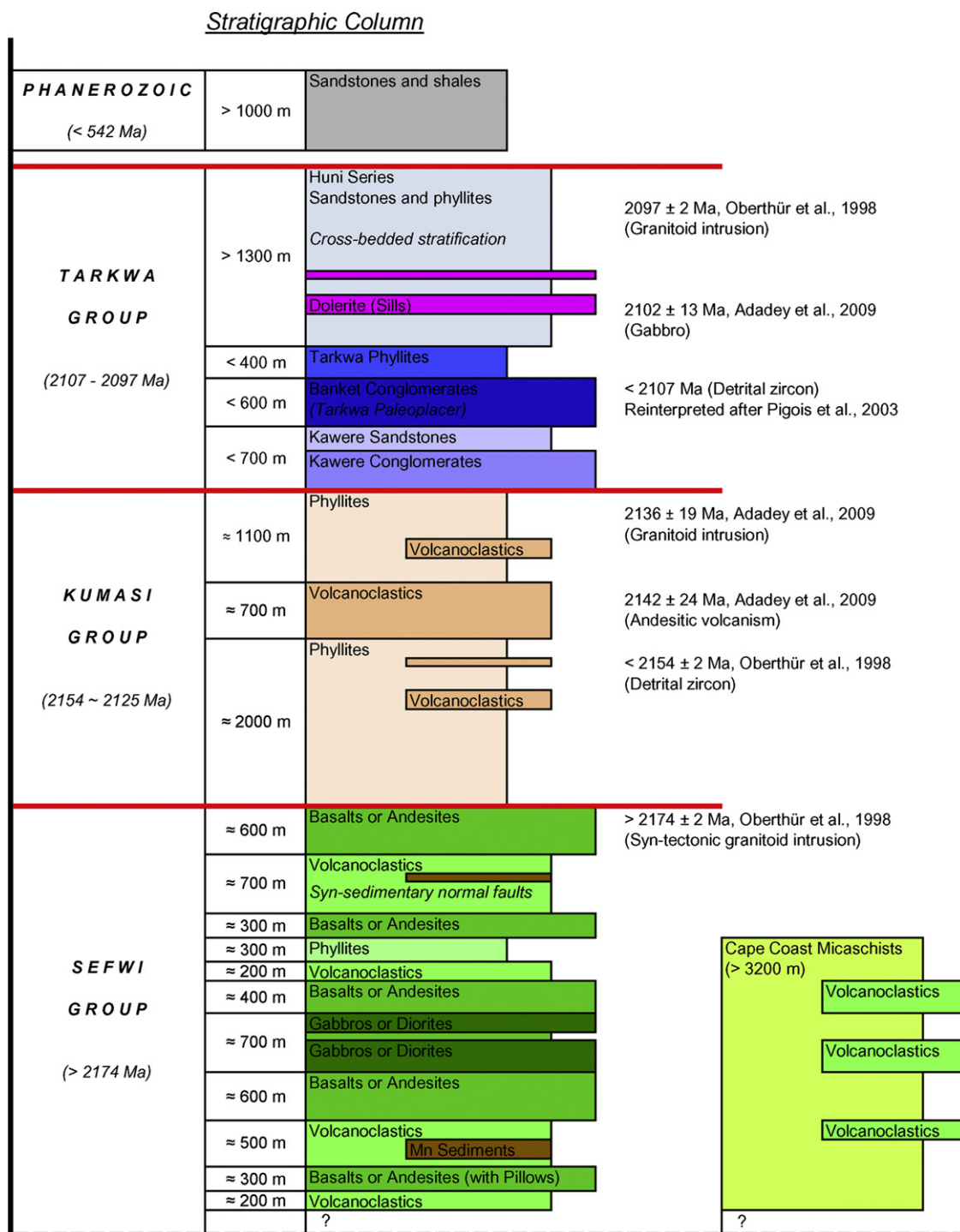
Fig. 8. New stratigraphy for the southwest of Ghana based on new data from this study and previous studies (Whitelaw, 1929; Junner, 1940; Kesse, 1985; Pigois et al., 2003; Adadey et al., 2009). Unit thicknesses are estimated from the map (Fig. 13). For clarity stratigraphic layers are labelled by their dominant lithology but could be subdivided into several sub-units.

affect both the S0–S1 and syn-D1 quartz veins and pegmatite intrusions (Fig. 11B). Radar data images bedding in the Sefwi Group that is folded by E-W trending F1 folds that are refolded by N-S trending F3 folds (Fig. 6).

The Kumasi Group phyllites in the Prestea, Bogoso and Pampe gold mines host isoclinal F3 folds from cm to m scale (Fig. 11C) that deform the bedding and a bedding parallel cleavage (S1). Quartz veins that are folded by F3 often show strongly boudinaged fold limbs.

In the Tarkwa Group, D3 is characterised by regional scale folds that deform relatively resistant lithological layers (S0) that are imaged by the combined digital elevation model and radiometric data (Fig. 4). At the outcrop scale, abundant parasitic F3 folds are observed with increases frequency and amplitude toward major F3 closures such as the Damang mines anticline (Fig. 11D). Major F3 folds are often open and low amplitude with NE-SW fold axis (Fig. 10A). In this region, subvertical S3 cleavages strike NE-SW parallel to the main regional Ashanti thrust fault.

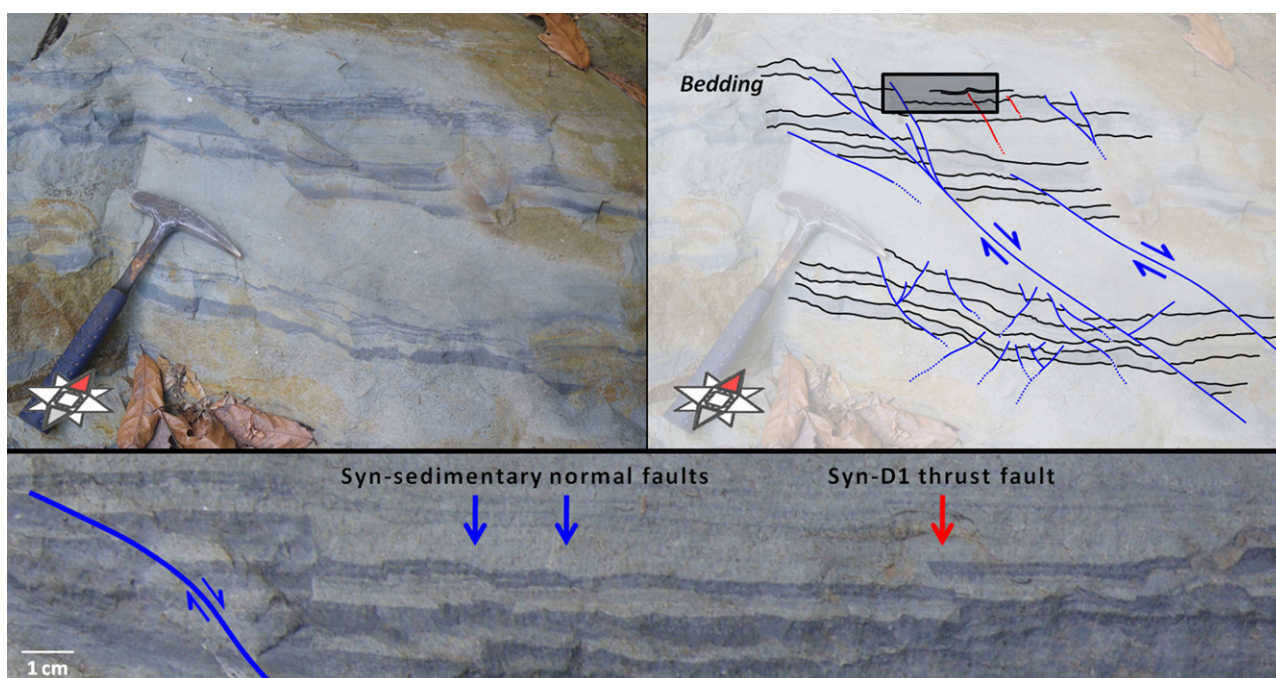**Fig. 9.** Photographs showing syn-sedimentary normal faults within Sefwi Group volcanoclastic sediments. Some of these faults do not affecting the youngest layers. Other faults show post-depositional reverse movement that could reflect the start of D1. The compass indicates both the north (in red) and the perspective. (For interpretation of the references to colour in this figure legend, the reader is referred to the web version of this article.)

4.2.4. D4

In the Bogoso gold mine on the western side of the Ashanti Belt, many small scale shear zones cross-cut F3 folds. Most of these shear zones show sinistral displacements and are interpreted to have formed in response to a later phase of deformation that we identify as D4. Major splays of the Ashanti Fault were also likely reactivated during sinistral shearing associated with D4. At Bogoso, one of these main Ashanti structures is mineralised within a 20–30 m thick band of graphitic phyllites and quartz breccias that separate Kumasi Group phyllites from the Sefwi Group basalts (Fig. 12). At the regional scale, magnetic images show at least two syn-D4 shear zone generations. The first one is oriented N030 and could correspond to the reactivation of D3 thrusts faults, such as the Ashanti Fault. The second is oriented N050 and cross-cuts earlier N030 shears, the F3 folds and the D3 thrusts within the Tarkwa Basin.

In the Wassa gold mine, within the Sefwi Group on the eastern border of the Tarkwaian sediments, a km scale F4 fold and associated parasitic folds overprint D3 faults and folds. F4 folds have only been observed at Wassa, although a subvertical S4 crenulation cleavage was found in many locations on both sides of the Tarkwa Basin. Intersection lineations between S3 and S4 cleavages and F4 folds axis give a plunge approximately 60° toward 260° (Fig. 10B). These characteristics correspond to a NNW-SSE shortening event that could be compatible with a sinistral shear reactivation of existing D3 regional thrust faults.

4.2.5. D5

The regional architecture of the Ashanti region was largely built during D1–D4 but has been modified by two subsequent deformation events that are observed to overprint D4 structures within the Sefwi, Kumasi and Tarkwa groups.

D5 is characterised by recumbent folds associated with a subhorizontal crenulation cleavage (Fig. 10B). These symmetrical open to tight folds have a wavelength varying between 5 m and 1 cm in the outcrops we studied. We note a great variability of amplitude between outcrops, varying with the lithology and orientation of previous structures. F5 folds were mainly observed in Wassa mine, in the NW of the belt (Pampe gold mine) and in the Tarkwaian sediments around Bogoso. In Damang, many quartz veins were subhorizontal and parallel to the S5 cleavage and formed either during or after D5.

4.2.6. D6

The final deformation event observed in the study area presents as a subvertical crenulation cleavage (S6) that defines open folds that affects subhorizontal S5 crenulation cleavage. S6 was observed in Tarkwaian sediments, in the Kumasi Group near the Akropong fault and in the Wassa gold mine. S6 is subvertical and NW-SE trending (Fig. 10B) approximately parallel to a series of reverse faults oriented NW-SE identified from the magnetic data. These faults cross-cut all Paleoproterozoic lithologies and earlier fault and cleavages. They were observed in the field at the Mpohor and Damang gold mines. The absence of observed overprinting of S6, and its relatively constant orientation, suggest that this D6 event was likely the last significant deformation event to affect the area.

4.3. Map

Field observations, combined with geophysical and radar data have allowed the construction of a new structural and geological model of the region (Fig. 13). This model describes the complex series of deformation events that affected the Sefwi Group basement and overlying Kumasi and Tarkwa groups during the Eburnean orogeny.

4.4. Sefwi Group D1 structures under the Tarkwa Basin

During the regional geophysical interpretation several significant differences between features observed in the digital elevation model, radiometric and radar data (which reflect near surface lithologies and structures, Dickson and Scott, 1997) compared to the aeromagnetic data over the Tarkwa Basin were observed. Orientation of regional magnetic trends are inconsistent with
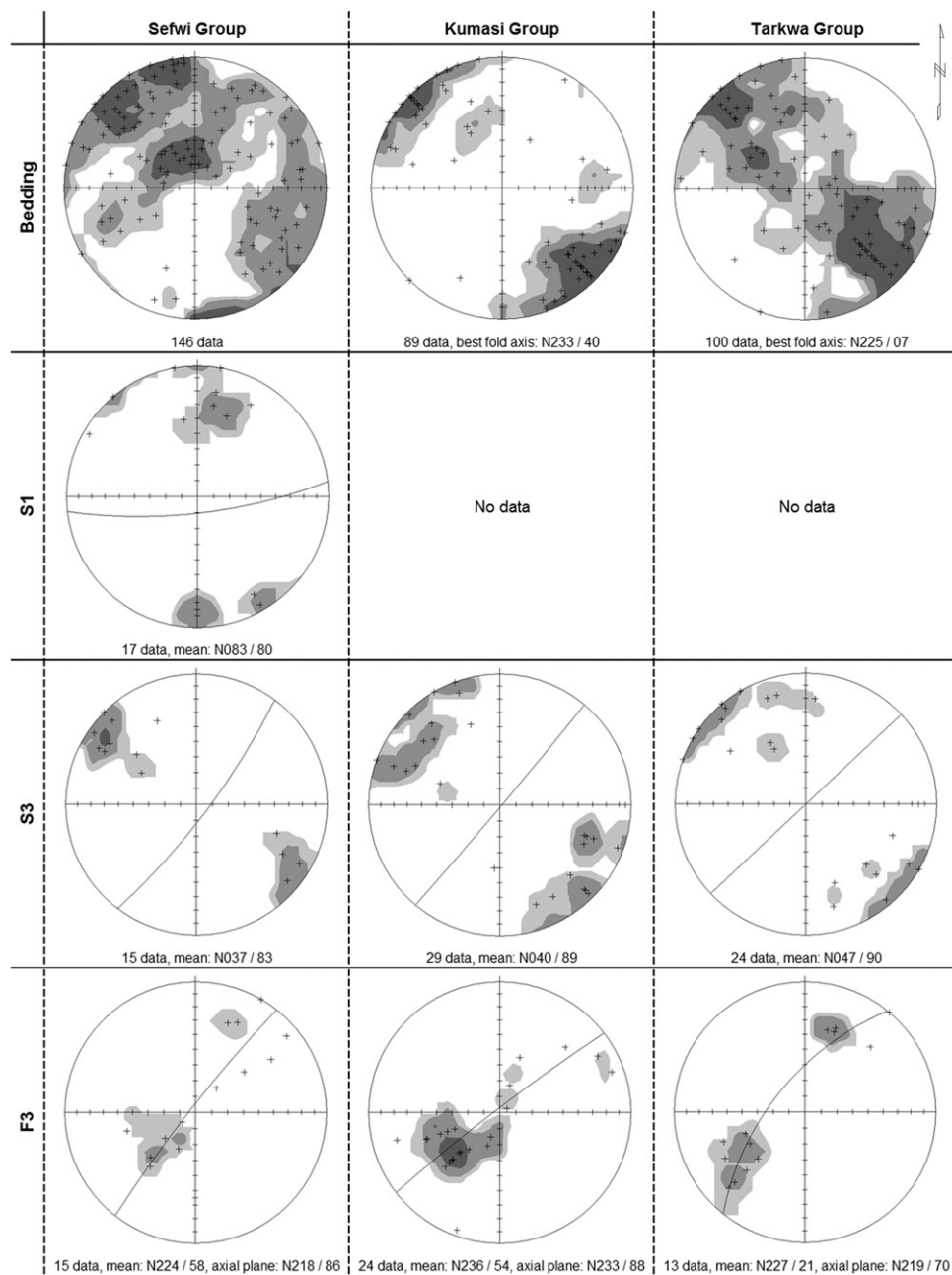
Fig. 10. Stereo-plot diagrams representing measurement distribution on equal area diagram (lower hemisphere), with density contours, for the three main rocks groups. (A) Distribution of the Kumasi Group and Tarkwaian sediments bedding poles are in good agreement with the F3 folding (and S3 cleavage orientations). In contrast the Sefwi Group bedding poles plots shows a wider dispersion resulting from the interference of multiple fold generations (mostly F1 and F3). Stereo-plots of poles to S1 confirm the presence of the earlier event (D1) affecting only the Sefwi Group. (B) D4 data are predominantly from the Wassa mine (Sefwi Group), although the S4 cleavage is also observed in the Kumasi Group and in the Tarkwa Group along the Ashanti Fault. S5 is sub-horizontal and consistent across each group. S6 corresponds to subvertical crenulation cleavage striking NW-SE.

observations made in the field (Tarkwaian bedding, S3 cleavage) and features imaged in the radiometric/radar data (e.g. F3 regional folds imaged in the combined radiometric/radar image do not appear in the magnetic data, Fig. 14).

Previous studies (Table 2) have estimated the total thickness of Tarkwaian sedimentary layers from 1000 to 3000 m. Assuming a maximum 3000 m depth for the Tarkwa Basin, several tests (Fig. 15) with various susceptibility contrasts were conducted using Noddy software (Jessell, 1981, 2001; Jessell and Valenta, 1996). The models suggest that in order to image structure in the buried Birimian basement, the Birimian must contain lithologies with approximately

5 times greater susceptibility than the overlying Tarkwa Group. Measurements of magnetic susceptibility within the Tarkwaian sediments show values that are indeed significantly lower (10 times or more) than the underlying Sefwi Group metavolcanics, with the exception of the few conglomerate layers. It is therefore possible that the magnetic data are not imaging structures within the Tarkwa Group but rather the structures in the underlying relatively magnetic Sefwi Group metasediments and metavolcanics. With this in mind we can interpret trends in the magnetic images as D1 structures in the Sefwi Group that formed prior to the deposition of the Tarkwaian sediments.
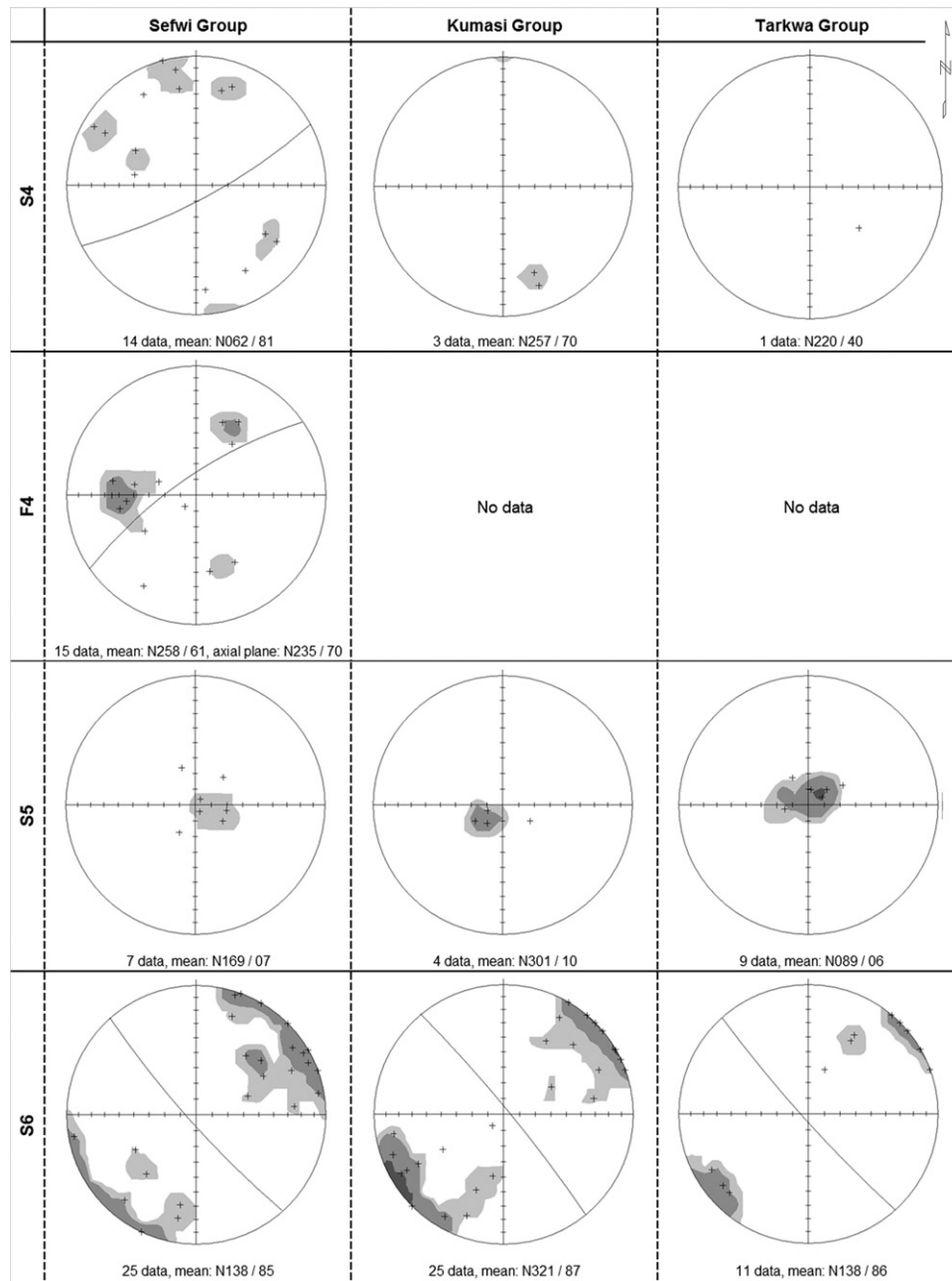
Fig. 10. (*Continued*)

4.5. Forward modelling

Forward-modelled geological cross-sections (Fig. 16) across the Ashanti Belt and Tarkwa Basin were constructed in order to understand and illustrate the structural relationship between the Birimian and Tarkwaian units produced during D1 and D3 shortening events. These sections are geologically consistent with the regional interpretation and the field observations. Forward-modelling was performed to ensure that geological cross-sections were also geophysically consistent with aeromagnetic, gravity and petrophysical data. Not all features within these models produce a perceptible geophysical contrast but are otherwise in agreement with the geological observations made within the study area.

Modelling was performed using Oasis Montaj GM-SYS software that utilises the algorithm of Talwani et al. (1959) and Talwani and Heirtzler (1964) to calculate the gravity and magnetic response of two-dimensional polygons. Construction of these integrated geological and geophysical models involved creating a traditional geological cross-section that was assigned values of magnetic susceptibility and density. The different fold trends in the Birimian and Tarkwaian units are represented in 2D by different fold wavelengths, amplitudes and positions of fold axes as they occur in the plane of the section. The geophysical response of this model was then calculated and compared to the observed aeromagnetic and gravity anomalies. The geometry and magnetic susceptibility/density values assigned to each rock package were then manipulated within geologically reasonable limits to improve the agreement between the model response and the observed response.

Magnetic susceptibility ranges for the modelled rock packages were based on field and laboratory susceptibility measurements
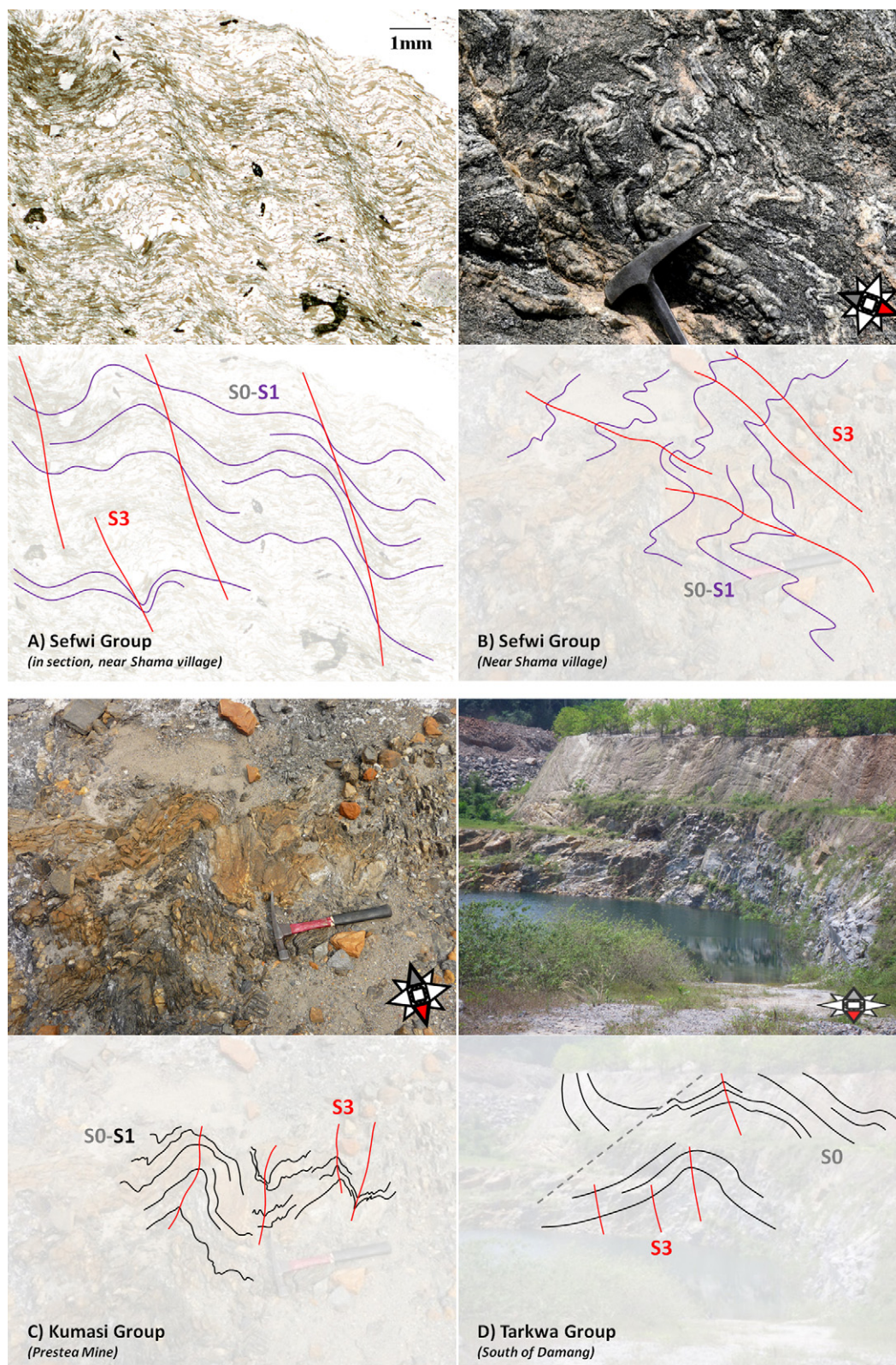
Fig. 11. Interpreted photographs showing examples of D3 deformation. (A) In the Sefwi Group, the S1 foliation defined by the alignment of biotite are partially transposed along the S3 cleavage. (B) Series of F3 ptygmatic folds at the same location. These F3 are folding a composite S0/S1 foliation and some quartz veins. (C) On the western side of the belt, F3 folds correspond to the first folding generation affecting the Kumasi Group sediments. (D) Parasitic open folds in the hinge of the Damang anticline in the Tarkwa Group. In all cases, S3 corresponds to a subvertical crenulation cleavage resulting from a NW–SE shortening. The compass indicates both the north (in red) and the perspective. (For interpretation of the references to colour in this figure legend, the reader is referred to the web version of this article.)
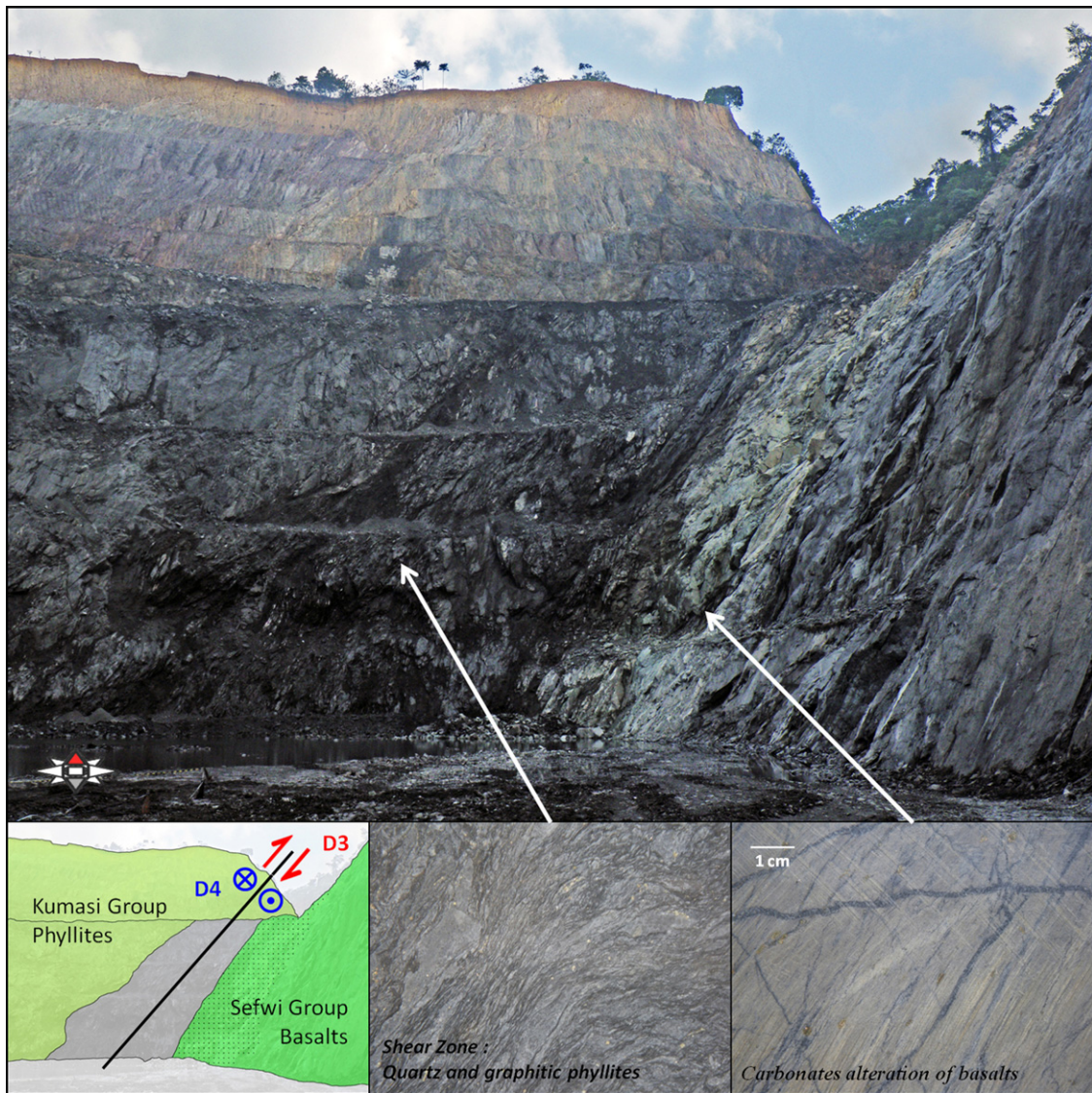
Fig. 12. Interpreted photographs showing the Ashanti Fault in Buesichem Pit (Bogoso Mine). The dark area in the middle corresponds to an approximately 20 m wide shear zone. This major structures separates the Kumasi Group phyllites from the Sefwi Group basalts. This shear zone operated as a thrust during D3 and was reactivated with a sinistral shear movement during D4. In the footwall, carbonatisation of the basalts (light green band) is synchronous with gold mineralisation. The compass indicates both the north (in red) and the perspectives view. Photographs of lithologies are not oriented. (For interpretation of the references to colour in this figure legend, the reader is referred to the web version of this article.)

(Fig. 7). The Kumasi Group metasediments (volcanoclastics and phyllites) show low susceptibility values (less than 10^{-3} SI) an order of magnitude lower than the Sefwi Group metavolcanics rocks (10^{-2} for basalts and gabbros) with anisotropies below 20%. High magnetic susceptibilities were mainly related to hydrothermal magnetite-rich layers within metasediments.

The Tarkwaian quartzite and phyllite display low susceptibilities (around 10^{-4} SI) related to rare detrital magnetite and biotite. However, some sandstone layers showed sedimentary structures that were defined by magnetite grains, resulting in local but important increases in magnetic susceptibility. Anisotropies within these Tarkwaian sediments were up to 56%. Magnetic variability observed within Tarkwaian conglomerates is likely caused by the presence of magnetic pebbles derived from the Sefwi Group metavolcanics rocks or granitoids. An average value of 10^{-3} SI has been used for modelling.

Granitoids displayed large ranges of magnetic susceptibility varying between 10^{-4} SI for the granites and 10^{-1} SI for the diorites. We assumed a mean value of 5×10^{-3} SI in the models. Generally,

more mafic units had higher magnetic susceptibilities. Anisotropy maxima are 8% for undeformed granitoids and 23% for the deformed granitoids.

Doleritic dykes correspond to one of the most magnetic lithologies in SW Ghana. They are magnetically isotropic (3%) with an average susceptibility approaching 2×10^{-2} SI. These dykes show strong remanent magnetisation of around 3 A/m, with declination of $59°$ and inclination of $-18°$.

The dominant magnetic response of the study area is located over the Tarkwa Basin where a complex series of high amplitude ($\approx$100 nT), linear anomalies that trend approximately parallel to the Ashanti Belt are imaged. These anomalies are predominantly produced by magnetic dolerite sills within the Tarkwa Group along with major faults within and along the margins of the Tarkwa Basin that host hydrothermal magnetite. In contrast, faults hosted entirely within the Birimian Supergroup such as the Akropong or the Twifo Praso faults do not produce significant magnetic anomalies. The strongest magnetic anomalies in the region lie to the east of the Tarkwa Basin within highly
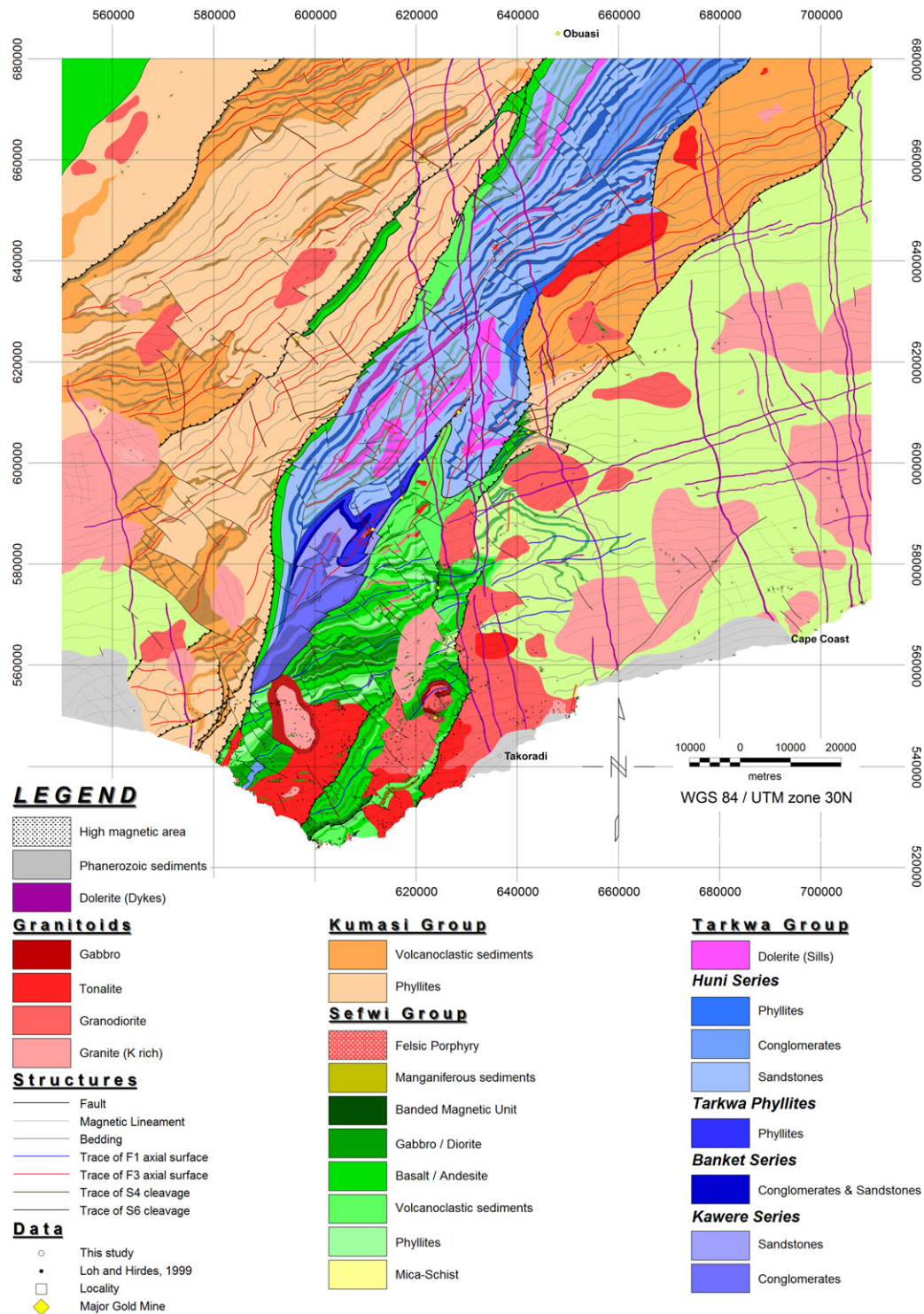
LEGEND

High magnetic area
Phanerozoic sediments
Dolerite (Dykes)

Granitoids
Gabbro
Tonalite
Granodiorite
Granite (K rich)

Structures
Fault
Magnetic Lineament
Bedding
Trace of F1 axial surface
Trace of F3 axial surface
Trace of S4 cleavage
Trace of S6 cleavage

Data
○ This study
• Loh and Hirdes, 1999
□ Locality
◇ Major Gold Mine

Kumasi Group
Volcanoclastic sediments
Phyllites

Sefwi Group
Felsic Porphyry
Manganiferous sediments
Banded Magnetic Unit
Gabbro / Diorite
Basalt / Andesite
Volcanoclastic sediments
Phyllites
Mica-Schist

Tarkwa Group
Dolerite (Sills)

Huni Series
Phyllites
Conglomerates
Sandstones

Tarkwa Phyllites
Phyllites

Banket Series
Conglomerates & Sandstones

Kawere Series
Sandstones
Conglomerates

Fig. 13. New lithological and structural interpretation based on the integration of new field observation, geophysical data and previous work. F1 folds built the regional geometries of the Sefwi Group metavolcanics. F3 folds are dominant in the Kumasi Group and Tarkwa Group sediments. D4 corresponds with a series of sinistral shear zones outlining the edge of the Tarkwaian sequence and cross-cutting it. S4 cleavage planes are oriented NE-SW and are observed around Bogoso/Prestea and Wassa. D5 is a minor event and is not represented as it is a subhorizontal cleavage. D6 is characterised by reverse faults oriented NW-SE.

magnetic Sefwi Group metavolcanics (Fig. 3). These rocks produce very high amplitude ($\approx$400 nT) broad anomalies over an area of 30 km^2 around Wassa mine. Other dominant magnetic features include NNW trending dolerite dykes that present as high amplitude ($\approx$100 nT) moderately remnant irregular linear anomalies.

The geometry and distribution of the magnetic lithologies were built into the forward-models based on the regional geophysical interpretation (Fig. 13), field observations, magnetic susceptibility data (Fig. 7) and gravity data (Table 5). Significant differences exist between the observed and calculated magnetic anomalies. These differences consist of low amplitude (<30 nT), short wavelength
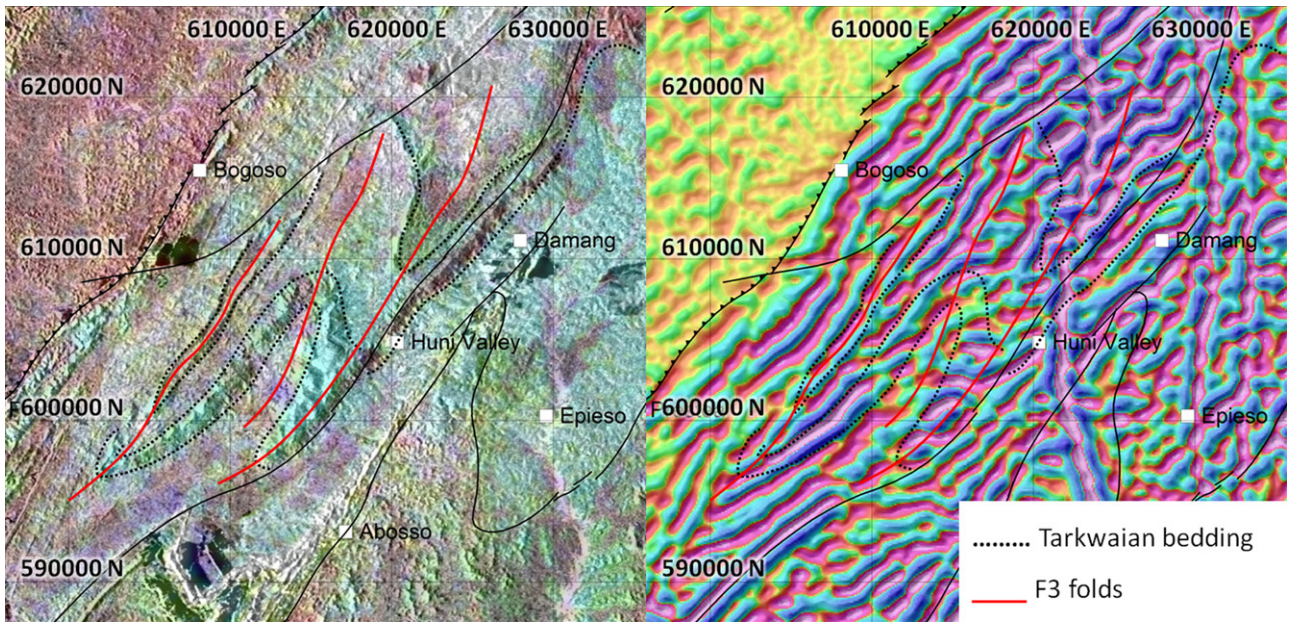
Fig. 14. Detailed comparison of radiometric (over HH radar polarisation) and magnetic data (RTP, first vertical derivative after automatic gain control). The magnetic trends do not correlate with bedding (S0) or S3 orientations observed in the Tarkwa Group that are well imaged in the radiometric data. These trends may correspond to older Sefwi Group lineaments (related to D1) beneath the Tarkwaian sediments. See Fig. 1 for location.
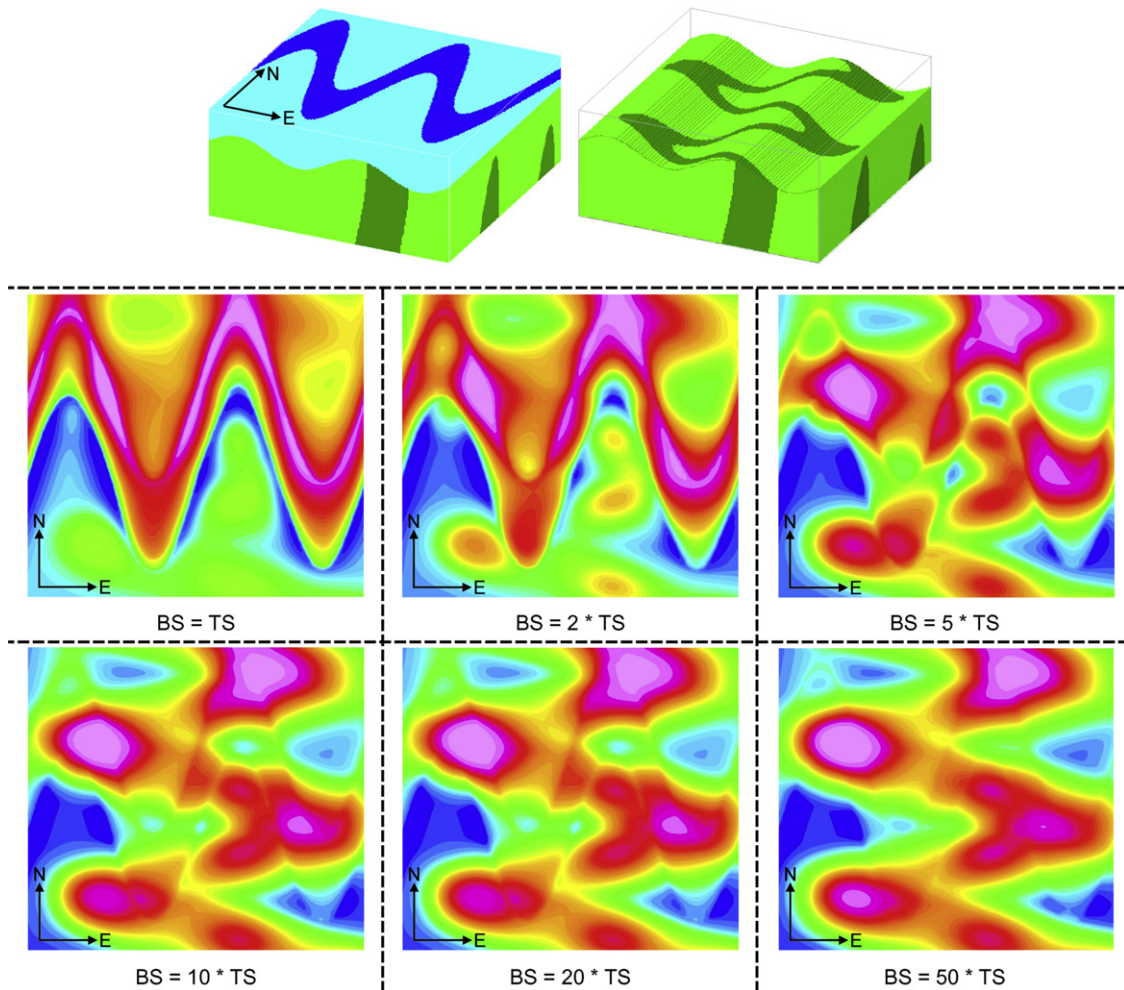
Fig. 15. Test of susceptibility impact of deep units on magnetic RTP image. These tests were conducted using Noddy software assuming a 3000 m maximum depth for the Tarkwa Basin with various susceptibility contrasts between the Sefwi Group (BS) and the Tarkwa Group (TS) susceptibilities. We note that the Sefwi Group structures (folds in this example) are imaged beneath the Tarkwa Basin when the Sefwi Group is at least 5 times more susceptible than the overlying Tarkwa Basin.

Fig. 16. Forward-modelled cross-sections across the Ashanti Belt. See Fig. 1 for location of these sections. These models highlight the mineralised Birimian/Tarkwaian contacts. Sefwi Group metavolcanics were highly deformed during the D1 and contrast with the more open syn-D3 folding in the Tarkwa Basin. Kumasi Group sediments on the western side of the Ashanti Fault were also deformed by D3. Major gold deposits have been geometrically projected onto their structural position.
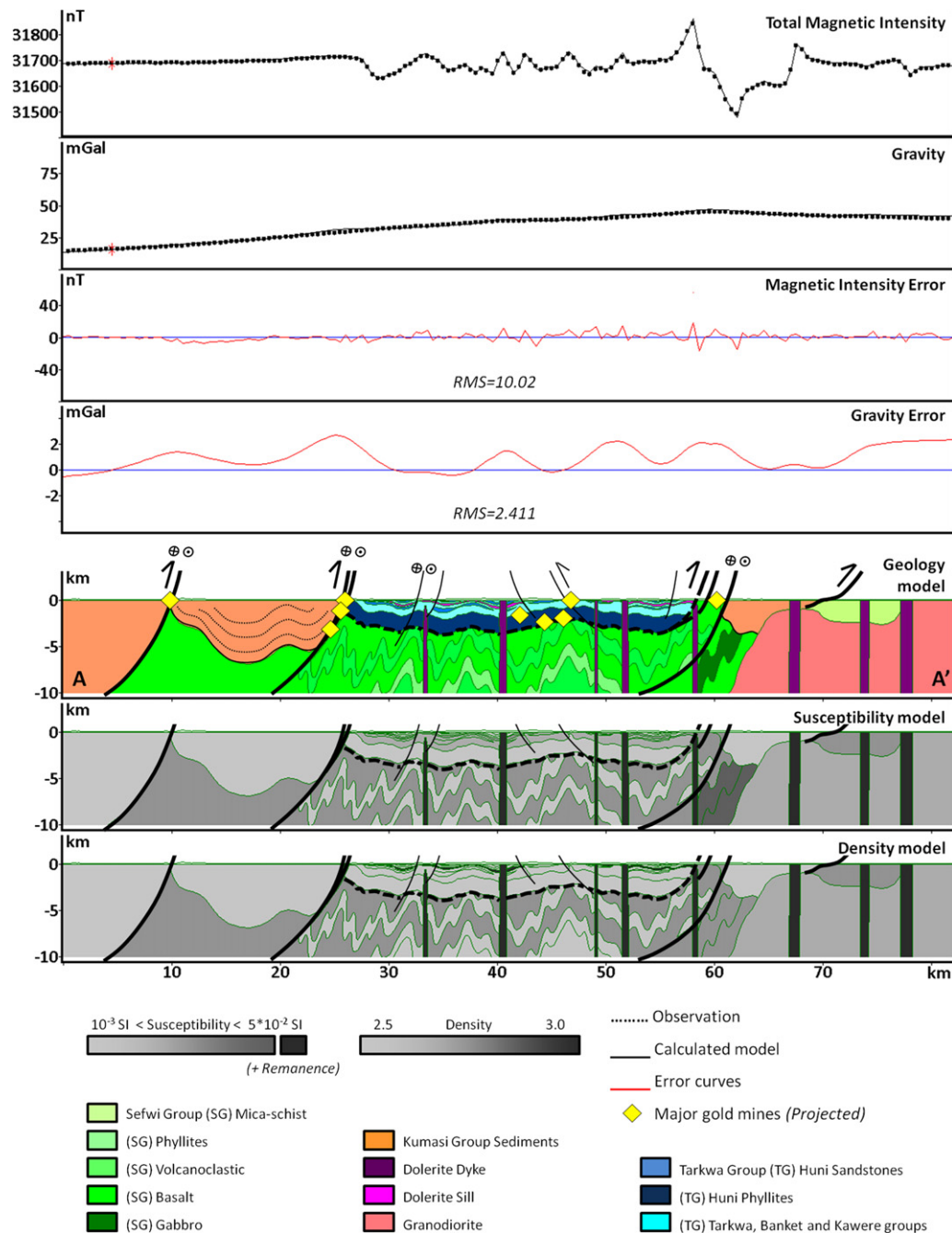
anomalies that were not able to be modelled using the previously described magnetic lithologies. Field observations indicate the presence of a 20–80 m thick weathered layer at the surface. This unit corresponds to thick lateritic successions that blanket most of the study area and contains highly variable magnetic susceptibilities related to the initial lithology and the degree of alteration and weathering. This lateritic horizon was modelled as a 50 m thick homogenous layer. It does not have any influence on the wavelengths at the scale of our modelling but it does reduce the amplitude of near-surface features. Given that we see this layer in the field it would be worse to ignore it altogether, even though we acknowledge that the thickness variations are unknown. Residual

magnetic anomalies reflect mostly the variations of susceptibility and thickness within this weathered layer.

Poor gravity coverage over the study area meant these data were only able to broadly constrain the depth of the relatively dense Sefwi Group basement. Density values (Table 5) used during the gravity modelling spanned the range proposed by Barritt and Kuma (1998) and Hastings (1982), using $3.0 \, \text{g/cm}^3$ for gabbros, $2.9 \, \text{g/cm}^3$ for basalts and dolerites, 2.8 for Eoeburnean granitoids, $2.7 \, \text{g/cm}^3$ for both volcanoclastics, phyllites and Eburnean granitoids and $2.65 \, \text{g/cm}^3$ for the micaschists. The surficial weathered layer was given a density of $2.6 \, \text{g/cm}^3$.
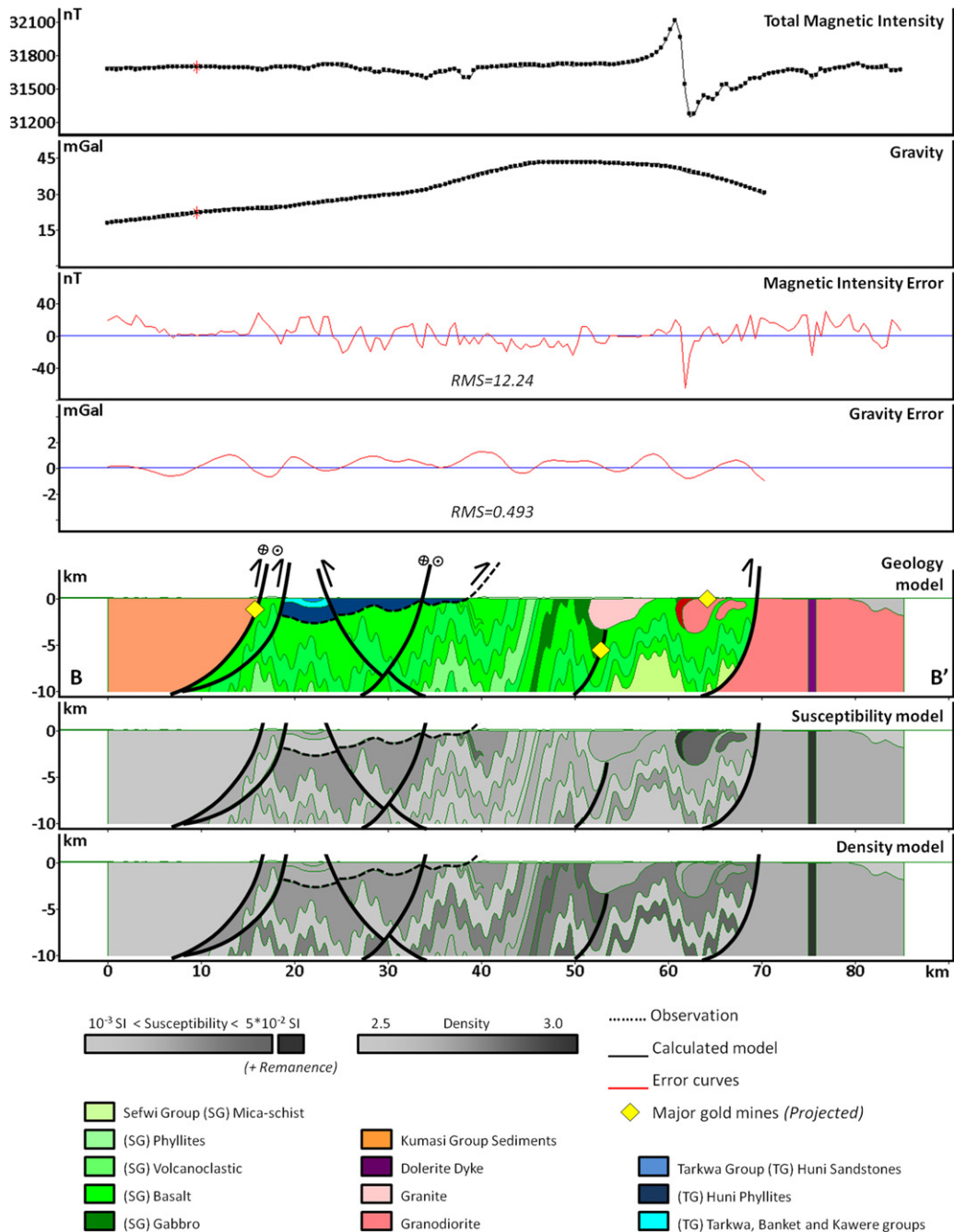
Fig. 16. (*Continued*)

Gravity anomalies are dominantly controlled by the distribution of the relatively dense metavolcanic group (Sefwi Group) and the less dense metasedimentary groups (Kumasi and Tarkwa groups). The small differences between the observed and modelled gravity anomalies are difficult to determine given the model resolution is higher than the gravity data.

5. Discussion

5.1. Eoeburnean phase (2187–2158 Ma)

Paleoproterozoic rocks of the southern Ashanti Belt were strongly deformed, mineralised and intruded by granitoids during the "Eburnean Orogeny" (Fig. 17). Previous interpretations of the regional tectonic evolution (e.g. Allibone et al., 2002a; Feybesse et al., 2006) suggest the Eburnean Orogeny initiated during the first phase of volcanic accretion and subduction that could correlate to D1 deformation. This hypothesis is in agreement with the interpretation of Sefwi Group mafic and ultramafic rocks as an ophiolitic suite (Attoh et al., 2006; Dampare et al., 2008). Our structural interpretation gives this accretionary phase a structural context whereby N-S shortening during D1 produced regional scale E-W trending folds within the Sefwi Group along with the intrusion of syn-tectonic granitoids (Fig. 13).

D1 occurred across south-eastern part of the Ashanti belt (Fig. 13) and below the Tarkwa Basin (Fig. 14). In Obuasi, Allibone et al. (2002a) described transfer faults and lineaments oriented E-W that were attributed to their NW-SE D2 shortening (our D3). The Obuasi deposit is mainly hosted within Kumasi Group metasediments. However, minor exposures of metavolcanics indicate the
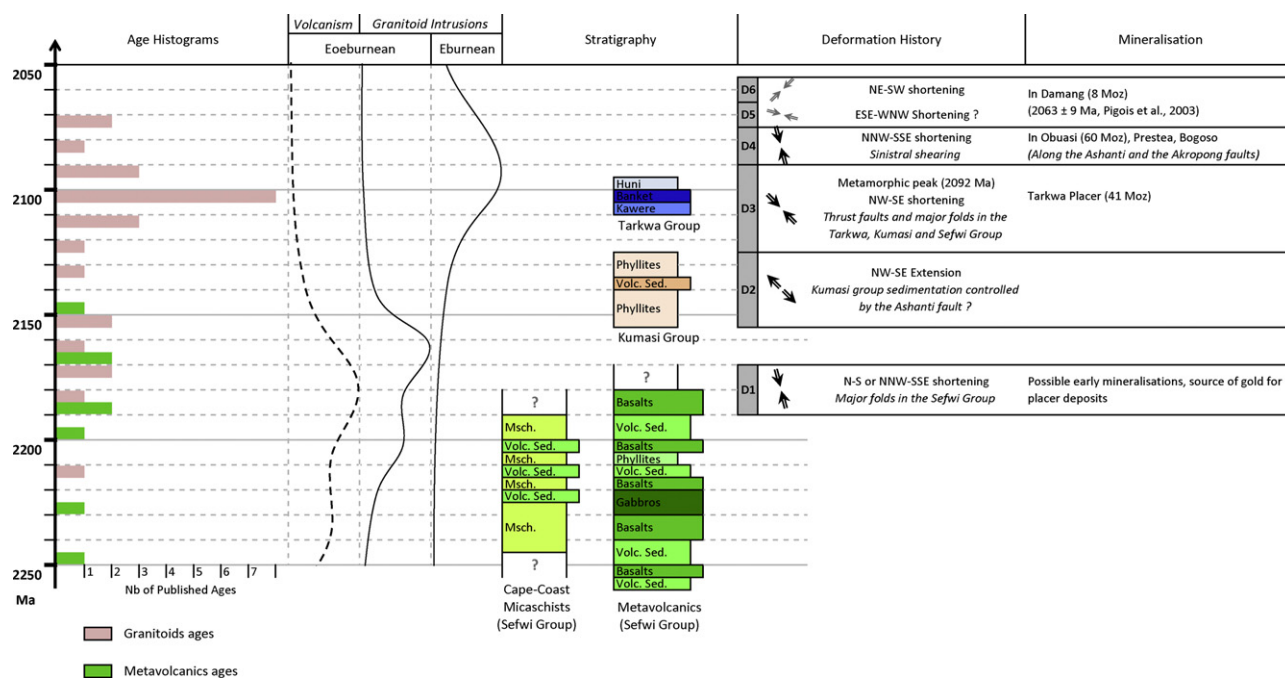
Fig. 17. Correlations between stratigraphic sequences, magmatism, deformations and mineralisations in south-west Ghana. The Cape Coast micaschists are not constrained by absolute or relative ages.

presence of the Sefwi Group basement at shallow depths. It is therefore possible that D1 deformation also affect this basement, developing E-W trending structures under a regional N-S shortening regime. Some existing D1 structures may have been reactivated during D3 (NW-SE shortening) and initiated as transfer faults such as those observed in the Obuasi mine. D1 deformation also explains the presence of the E-W lineaments reported by Allibone et al. (2002a, Fig. 5, p. 72).

Deformed granitoids such as those found in Sekondi (Loh et al., 1999), help constrain the timing of this Eoeburnean deformation phase (D1). Linear magnetic anomalies in this granitoid are sub-parallel to the dominant S1 in the Birimian micaschist. Consequently, we suggest that this intrusion, dated at 2174 ± 2 Ma (Oberthür et al., 1998), is contemporaneous with D1. The undeformed Dixcove tonalite suggests that peak D1 deformation occurred before 2171 ± 2 Ma (Hirdes et al., 1992).

5.2. Kumasi Group deposition (2154–2125 Ma)

Eoeburnean tectonism produced magmatism between approximately 2187 and 2158 Ma and deformation that occurred before 2171 Ma. The Eoeburnean event predates deposition of the Kumasi Group sediments, and was only observed within the Sefwi Group basement. This places the deposition and lithification of the Kumasi Group between D1 and D3.

The Kumasi Group within the Kumasi and the Akyem Basins (Fig. 1) formed under an extensional regime during D2 (Stage 4 of Feybesse et al., 2006), where major faults (e.g. Ashanti, Akropong faults) behaved as primary basin forming structures and possible detachment surfaces prior to reactivation as D3 thrust faults. Direct evidence for an extensional origin for the Ashanti Fault is obscured by the strong overprinting (D3 thrust and D4 strike-slip movement, Allibone et al., 2002a). However, the opening of the Kumasi Basin required the generation of an extensional fault architecture that have been favourably orientated to undergo reactivation during D3 shortening.

The strong magnetic and gravity contrasts across the Ashanti Fault (Figs. 5 and 16) suggest large amounts of vertical displacement

have juxtaposed rocks with contrasting petrophysical properties. The absence of metamorphic gradient across the Ashanti Fault is not consistent with significant vertical thrust movement during D3 shortening. Consequently, we propose the Ashanti Fault was initiated as a half-graben during D2 deformation. Evidence of a widespread D2 extensional phase has also been identified in northwest Ghana, where De Kock et al. (2011) proposed a significant period of rifting between 2148 Ma and 2125 Ma. This timing is consistent with the deposition of the Kumasi Group between 2154 ± 2 Ma (youngest U/Pb age on zircon found by Oberthür et al., 1998) and 2136 ± 19 Ma (Granitoid intrusion, U/Pb on zircon, Adadey et al., 2009).

Adadey et al. (2009, p. 80) reported an early deformation in the Kumasi Group that was interpreted as pre-diagenetic slumping. This deformation is characterised by rare isoclinal fold-like structures that are coaxial with deformation that affected both the Birimian and Tarkwaian units (our D3). These folds could have resulted from Eoeburnean D3 deformation that intitiated after the deposition of the Kumasi Group and before the Tarkwaian sedimentation. This hypothesis is also consistent with observations of an early bedding parallel cleavage in the Kumasi Group by Allibone et al. (2002a). This layer parallel fabric is interpreted it as resulting from bedding-parallel shearing (their D1, our D3) during the early Eoeburnean Orogeny that is absent in the Tarkwa Group.

5.3. Tarkwa Group deposition (2107–2097 Ma)

The Tarkwa Group occurs as a synclinal erosional remnant overlying the metavolcanic Sefwi Group in the Ashanti Belt. The timing and nature of the contact between the Tarkwa Group and the Birimian Supergroup is not clear, but probably represents an unconformity or faulted contact. Both margins of the preserved Tarkwa Basin are represented by major faults. These faults may have been important during the early evolution of the Tarkwa Basin; however, strong reactivation obscures their early history.

The presence of early deformation in the Kumasi Group metasediments is an indicator of the initiation of the Eoeburnean Orogeny before the Tarkwaian deposition. However, the majority

of Eburnean deformation occured after the Tarkwaian deposition and after intrusions of metagabbro sills within the Tarkwa Group at 2102 ± 13 Ma (U/Pb on zircon, Adadey et al., 2009). It is therefore possible that the major D3 transcurrent structures such as the Ashanti Fault initiated before the Tarkwa Group sedimentation. Reactivation of the D2 Ashanti detachment fault with transcurrent movement may occurred at the start of Eburnean D3 shortening and would have controlled the Tarkwaian deposition on its western side. Similar faults should exist on the eastern side of the basin, but are not observed due to intense overprinting.

This hypothesis of a Tarkwa Basin bordered by two major transcurrent faults is consistent with the presence of conglomerate and sandstones beds that alternate in the first 1000 meters of the Tarkwa Group. This syn-orogenic molasse and the presence of placer deposits along paleochannels (Sestini, 1973) suggest short transport distances in a shallow water environment that has also been proposed by Baratoux et al. (2011) in Burkina Faso and in the Abitibi or Yilgarn cratons within similar intra-orogenic basins (Eriksson et al., 1994).

5.4. Eburnean Phase (2125–1980 Ma)

The post-Tarkwaian Eburnean event is clearly visible and well preserved in the field. D3 deformed the entire crustal pile made up of the Birimian Supergroup and the Tarkwa Group. Regional mapping shows a series of kilometric scale F3 folds in both the Kumasi and Tarkwa groups metasediments related to NW-SE shortening (Fig. 13). D3 deformation in the Sefwi Group is associated with regional folding of the S1 foliation. An example of this relationship is found at Shama beach, where F3 ptygmatic folds affect bedding and a melt rich S1 foliation (Fig. 11B). According to Milési et al. (1992) and Feybesse et al. (2006) D3 shortening was responsible for creating many of the major thrust faults as well as regional folding (e.g. the Ashanti and Akropong faults). The distribution of these thrusts is probably related to reactivation of the existing D2 extensional architecture. D3 thrusting along the Ashanti Fault is related to the metamorphic peak (650 °C and 6 kbar; John et al., 1999), dated at 2092 ± 3 Ma (Oberthür et al., 1998). D3 spans from approximately 2125 Ma to over 2092 Ma with major folding occurring after the Tarkwaian deposition at around 2097 Ma.

Observations along the Ashanti Fault zone around Prestea and Bogoso gold mines show an increase in the intensity of F3 folding on the western sides of fault contacts between Kumasi Group phyllites (west) and Tarkwa Group phyllites (east) (Fig. 12C and D). This asymmetry suggests strain was being preferentially partitioned into the Kumasi Group phyllites. On the other side of the belt, an angular unconformity between the Kumasi and Tarkwa groups sediments is imaged in the geophysical data. This unconformity suggests that Tarkwaian sediments may have been displaced eastward during D3 accommodated by a low angle thrust or decollement at depth.

Our mapping shows syn-D4 shear zones that both bound and cross-cut Tarkwaian sediments. Some of these structures overprint regional F3 folds. D4 structures including the Ashanti and Akropong faults, along with other syn-D3 thrust faults were reactivated via sinistral strike-slip movement during D4 (Allibone et al., 2002b). Two major F4 folds observed in the Wassa and Obuasi gold mines could have been developed during shearing (Allibone et al., 2002a). By the end of the D4 (NNE-SSW shortening) the regional architecture was created and only weakly modified by successive events. D5 is characterised by small scale recumbent folds, resulting from a WNW -ESE shortening (Tunks et al., 2004). The final D6 event is associated with NW-SE oriented reverse faults identified in the field and in the geophysical data to overprint all earlier generation structures. D4, D5 and D6 deformation occurred approximately

from 2092 Ma to 2063 Ma (estimated age of the mineralisation in Damang, Pigois et al., 2003)

Timing of the Eburnean Orogeny plutonism could be constrained by granitoid intrusion at 2136 ± 19 Ma (Adadey et al., 2009) and at 2116 ± 2 Ma (Hirdes et al., 1992) for its beginning, post or syn-sedimentation into the Kumasi Group, pre-sedimentation in the Tarkwa Group. Some undeformed potassium rich granitoid intrusions that overprint all previous structures could be related with the late stages of the Eburnean orogeny. However, their ages have not been determined precisely yet (1973 ± 75 Ma, Pb/Pb date on whole rock, Taylor et al. (1992) and 1978 ± 37 Ma, Ar/Ar date on amphibole, Feybesse et al. (2006)).

5.5. Implications for Au deposits

5.5.1. Timing of gold mineralisation and metamorphism

Gold mineralisation in the southwest of Ghana is divided in to two main hydrothermal events. The first period corresponds to the major gold deposits found along the Ashanti Fault (Prestea, Bogoso, Obuasi, Fig. 1) and the Akropong fault (Ayanfuri, Pampe, Obuasi, Fig. 1). Fluid inclusion studies on mineralised quartz veins suggest low temperature and pressure homogenisation conditions for all major deposits. These factors suggest that mineralisation occurred after the metamorphic peak (related to D3) and probably synchronously with D4 shearing (Oberthür et al., 1994, 1997).

The second hydrothermal event is associated with mineralisation along the Sefwi/Tarkwa groups contact on the eastern side of the belt (Abosso-Damang Mine, Fig. 1) during D6. This mineralisation is dated at 2063 ± 9 Ma (U/Pb on xenotime) by Pigois et al. (2003) and represents the youngest known deposit in the region. The greenschist conditions for its formation are equivalent to the deposits found along the Ashanti Fault.

An additional mineralisation event is required to explain the origin of the Tarkwaian paleoplacer. This placer was developed during Tarkwaian deposition at the start of D3 and has long been considered to be sourced from aforementioned Sefwi Group gold deposits. This correlation is based on similar fluid inclusion chemistry between Tarkwaian quartz pebbles and Birimian (Sefwi Group) quartz veins (Klemd et al., 1993). However, the maximum depositional age of the Tarkwaian sediments (2107 Ma) and their deformation during D3 is inconsistent, with placer deposits derived from mineralisation hosted in the Sefwi Group that formed during D4–D6 (Milesi et al., 1991; Eisenlohr, 1992; Hirdes and Nunoo, 1994). The Tarkwaian paleo-placer therefore needs to be derived from earlier sources of gold.

As shown by our study, the Sefwi Group, in the south east of the belt, displays strong pre-Tarkwaian deformation associated with significant plutonism. Although no syn-D1 deposits have been described in southwestern Ghana, they may represent early sources of gold that supplied the Tarkwaian Paleoplacer along with gold that was remobilised in shear zones during the Eburnean II orogenic phase. Possible Eoeburnean mineralised quartz veins have been suggested by Sestini (1973) and Kesse (1985). An Eoeburnean gold source is also in agreement with paleoflow indicators that suggest the Banket conglomerates were sourced from Birimian schist and volcano-sedimentary rocks to the east of the Ashanti Belt.

5.5.2. Regional distribution of the mines

If we look at the distribution of gold mines in the study area (Figs. 13 and 16A), several deposits are located at or close to the margin of the Tarkwaian sediments. Prestea, Bogoso and Obuasi on the western side are located along a 500 m thick faulted and sheared area lying the contact (Ashanti Fault). On the eastern side of the belt, the Abosso-Damang deposits appear to lie directly on the Sefwi/Tarkwa groups contact.

In accordance with Feybesse et al. (2006), we suggest that D3 shortening lead to the development of a low angle decollement beneath the Tarkwa Basin that was responsible for transporting the Tarkwa Group to the east. Such a structure would be favourable for fluid circulation and gold mineralisation, and would explain the distribution of many major gold deposits that are located on the margins of the Tarkwaian sediments. Further, gold along this structure would also be a possible source of gold for shear zone hosted deposits remobilised during D4.

6. Conclusions

This paper presents a new structural interpretation of the southern Ashanti Belt in southwestern Ghana. Utilising field observations, magnetic, radiometric, gravity and radar data, we distinguish at least 6 distinct deformation events that occurred in two phases (Eoeburnean and Eburnean) during the Paleoprotero-zoic (Fig. 17). We also establish a new stratigraphy (Fig. 8) for the Birimian Supergroup (Sefwi Group and Kumasi Group). Our map (Fig. 13) and sections (Fig. 16) display a series of tight F1 folds that only affected the Sefwi Group basement. This group was overlain by the Kumasi Group during D2 extension and by the Tarkwa Basin that developed at the start of D3 shortening controlled by major transcurrent faults such as the Ashanti Fault.

Significant gold mineralisation may have occurred during both Eoeburnean and Eburnean phases. Quartz veins that formed during the early phase (Eoeburnean) may also represent the source of the gold rich quartz pebbles found in the Tarkwa paleoplacer. We suggest that many hydrothermal gold deposits in the Ashanti region were formed by remobilisation and concentration of syn-D1 gold along D4 shear-zones and the contact zones between the Birimian and Tarkwaian units during the Eburnean orogeny.

References

Adadey, K., Clarke, B., Théveniaut, H., Urien, P., Delor, C., Roig, J.Y., Feybesse, J.L., 2009. Geological map explanation—Map sheet 0503 B (1:100 000), CGS/BRGM/Geoman. Geological Survey Department of Ghana (GSD). No MSSP/2005/GSD/5a.

Agyei Duodu, J., Loh, G.K., Boamah, K.O., Baba, M., Hirdes, W., Toloczyki, M., Davis, D.W., 2009. Geological map of Ghana 1:1 000 000. Geological Survey Department of Ghana (GSD).

Allibone, A., McCuaig, T.C., Harris, D., Etheridge, M., Munroe, S., Byrne, D., 2002a. Structural controls on gold mineralization at the Ashanti Gold Deposit, Obuasi, Ghana. Society of Economic Geologists (Special Publication) 9, 65–93.

Allibone, A., Teasdale, J., Cameron, G., Etheridge, M., Uttley, P., Soboh, A., Appiah-Kubi, J., Adanu, A., Arthur, R., Mamphey, J., Odoom, B., Zuta, J., Tsikata, A., Pataye, F., Famiyeh, S., Lamb, E., 2002b. Timing and structural controls on gold mineralization at the Bogoso Gold Mine, Ghana, West Africa. Economic Geology 97, 949–969.

Attoh, K., Evans, M.J., Bickford, M.E., 2006. Geochemistry of an ultramafic-rodingite rock association in the Paleoproterozoic Dixcove greenstone belt, southwestern Ghana. Journal of African Earth Sciences 45, 333–346.

Baratoux, L., Metelka, V., Naba, S., Jessell, W.M., Gregoire, M., Ganne, J., 2011. Juvenile paleoproterozoic crust evolution during the Eburnean orogeny (−2.2-2.0 Ga), western Burkina Faso. Precambrian Research 191, 18–45.

Barritt, S.D., Kuma, J.S., 1998. Constrained gravity models and structural evolution of the Ashanti Belt, southwest Ghana. Journal of African Earth Sciences 26 (4), 539–550.

Baer, P., Riegel, W., 1980. Les microflores des séries Paléozoiques du Ghana (Afrique occidentale) et leurs relations paléofloristiques. Geological Science Bulletin 27, 39–58.

Blenkinsop, T.G., Schmidt Mumm, A., Kumi, R., Sangmor, S., 1994. Structural geology of the Ashanti Gold Mine. Geologisches Jahrbuch D 100, 131–153.

Bonhomme, M., 1962. Contribution à l'étude géochronologique de la plate-forme de l'Ouest Africain. Ann. Fac. Sci. Univ. Clermont-Ferrand Géol. Minéral. 5, 62.

Bowell, R.J., Foster, R.P., Stanley, C.J., 1990. Telluride mineralization at Ashanti gold mine, Ghana. Mineralogical Magazine 54, 617–627.

Chaloner, W.G., Mensah, M.K., Crane, M.D., 1974. Non-vascular land plants from the Devonian of Ghana. Palaeontology 17 (4), 925–947.

Clark, D.A., 1997. Magnetic petrophysics and magnetic petrology: aids to geological interpretation of magnetic surveys. AGSO Journal of Australian Geology and Geophysics 17 (2), 83–103.

Crow, A.T., 1952. The rocks of the Sekondi Series of the Gold Coast. Gold Coast Geological Survey 18, 68.

Dampare, S.B., Shibata, T., Asiedu, D.K., Osae, S., Banoeng-Yakubo, B., 2008. Geochemistry of Paleoproterozoic metavolcanic rocks from the southern Ashanti volcanic belt, Ghana: petrogenetic and tectonic setting implications. Precambrian Research 162, 403–423.

Davis, D.W., Hirdes, W., Schaltegger, U., Nunoo, E.A., 1994. U–Pb age constraints on deposition and provenance of Birimian and gold-bearing Tarkwaian sediments in Ghana, West Africa. Precambrian Research 67, 89–107.

De Kock, G.S., Armstrong, R.A., Siegfried, H.P., Thomas, E., 2011. Geochronology of the Birim Supergroup of the West African craton in the Wa-Bolé region of west-central Ghana: implications for the stratigraphic framework. Journal of African Earth Sciences 59, 1–40.

Dickson, B.L., Scott, K.M., 1997. Interpretation of aerial gamma-ray surveys—adding the geochemical factors. AGSO Journal of Australian Geology and Geophysics 17 (2), 187–200.

Eisenlohr, B.N., 1992. Conflicting evidence on the timing of mesothermal and paleoplacer gold mineralisation in early Proterozoic rocks from southwest Ghana, West Africa. Mineralium Deposita 27, 23–29.

Eisenlohr, B.N., Hirdes, W., 1992. The structural development of the early Proterozoic Birimian and Tarkwaian rocks of southwest Ghana, West Africa. Journal of African Earth Sciences 14 (3), 313–325.

Eriksson, K.A., Krapez, B., Fralick, P.W., 1994. Sedimentology of Archean greenstone belts; signatures of tectonic evolution. Earth-Science Reviews 37, 1–88.

Feybesse, J.L., Billa, M., Guerrot, C., Duguey, E., Lescuyer, J.L., Milési, J.P., Bouchot, V., 2006. The paleoproterozoic Ghanaian province: geodynamic model and ore controls, including regional stress modeling. Precambrian Research 149, 149–196.

Griffis, R.J., Barning, K., Agezo, F.L., Akosah, F.K., 2002. Gold Deposits of Ghana. Minerals Commission, Accra, Ghana, p. 438.

Gunn, P.J., Maidment, D., Milligan, P.R., 1997. Interpreting aeromagnetic data in areas of limited outcrop. AGSO Journal of Australian Geology and Geophysics 17 (2), 175–185.

Hastings, D.A., 1982. On the tectonics and metallogenesis of West Africa, A model incorporating new geophysical data. Geoexploration 20, 295–327.

Hein, K.A.A., 2010. Succession of structural events in the Goren greenstone belt (Burkina Faso): implications for West African tectonics. Journal of African Earth Sciences 86, 77–89.

Hirdes, W., Davis, D.W., 1998. First U–Pb zircon age of extrusive volcanism in the Birimian Supergroup of Ghana/West Africa. Journal of African Earth Sciences 27 (2), 291–294.

Hirdes, W., Davis, D.W., Eisenlohr, B.N., 1992. Reassessment of proterozoic granitoid ages in Ghana on the basis of U/Pb zircon and monazite dating. Precambrian Research 56, 89–96.

Hirdes, W., Nunoo, B., 1994. The proterozoic paleoplacers at Tarkwa Gold Mine, SW Ghana: sedimentology, mineralogy, and precise age dating of the main reef and west reef, and bearing of the investigations on source area aspects. Geologisches Jahrbuch D 100, 247–311.

Hünken, U., Klemd, R., Olesch, M., 1994. Fluid inclusions in quartz-pebbles of proterozoic tarkwaian conglomerates in Ghana. Geologisches Jahrbuch D 100, 313–341.

Jessell, M.W., 1981. Noddy—an interactive map creation package. M.Sc. Thesis, University of London, England, 49 p.

Jessell, M.W., Valenta, R.K., 1996. Structural geophysics: integrated structural and geophysical mapping. In: DePaor, D. (Ed.), Structural Geology and Personal Computers. Elsevier, Oxford, pp. 303–324.

Jessell, M.W., 2001. Three-dimensional geological modelling of potential-field data. Computers and Geosciences 27, 147–157.

John, T., Klemd, R., Hirdes, W., Loh, G., 1999. The metamorphic evolution of the Paleoproterozoic (Birimian) volcanic Ashanti belt (Ghana, West Africa). Precambrian Research 98, 11–30.

Junner, N.R., 1935. Gold in the Gold Coast. Gold Coast Geological Survey, Memoir No. 4, 76 p.

Junner, N.R., 1940. Geology of the Gold Coast and Western Togoland. Gold Coast Geological Survey, Memoir No. 11, 40 p.

Kalsbeek, F., Frei, D., Affaton, P., 2008. Constraints on provenance, stratigraphic correlation and structural context of the Volta basin, Ghana, from detrital zircon geochronology: an Amazonian connection? Sedimentary Geology 212, 86–95.

Kesse, G.O., 1985. The Mineral and Rock Resources of Ghana. A.A. Balkema Publishers, p. 610.

Kitson, A.E., 1918. Annual Report for 1916/17. Gold Coast Geological Survey, Accra, Ghana.

Kitson, A.E., 1928. Provisional geological map of the Gold Coast and Western Togoland, with brief descriptive notes thereon. Gold Coast Geological Survey, Accra, Ghana.

Klein, E.L., Moura, C.A.V., Pinheiro, B.L.S., 2005. Paleoproterozoic crustal evolution of the São Luis Craton, Brazil: evidence from zircon geochronology and Sm–Nd isotopes. Gondwana Research 8 (2), 177–186.

Klein, E.L., Luzardo, R., Moura, C.A.V., Armstrong, R., 2008. Geochemistry and zircon geochronology of paleoproterozoic granitoids: further evidence on the magmatic and crustal evolution of the São Luís cratonic fragment, Brazil. Precambrian Research 165, 221–242.

Kleinschrot, D., Klemd, R., Brocker, M., Okrusch, M., Franz, L., Schmidt, K., 1993. The Nsuta manganese deposit, Ghana: geological setting, ore-forming process and metamorphic evolution. Zeitschfirt fuer Angewandte Geologie 39, 135–155.

Kleinschrot, D., Klemd, R., Brocker, M., Okrusch, M., Franz, L, Schmidt, K., 1994. Protores and country rocks of the Nsuta manganese deposit. Neues Jahrbuch Mineral 168, 67–108.

Klemd, R., Hirdes, W., Olesch, M., Oberthür, T., 1993. Fluid inclusions in quartz-pebbles of the gold-bearing Tarkwaian conglomerates of Ghana as guides to their provenance area. Mineralium Deposita 28, 334–343.

Kutu, J.M., 2003. Structure, deformation and mineralization of Konongo Mines in the Ashanti Gold Belt of Ghana. PhD Thesis, Univeristy of Ghana.

Lahti, I., Karinen, T., 2010. Tilt derivative multiscale edges of magnetic data. The Leading Edge 23 (2), 116–118.

Ledru, P., Johan, V., Milési, J.P., Tegyey, M., 1994. Markers of the last stages of the Palaeoproterozoic collision: evidence for a 2 Ga continent involving circum-South Atlantic provinces. Precambrian Research 69, 169–191.

Leube, A., Hirdes, W., Mauer, R., Kesse, G.O., 1990. The early proterozoic Birimian supergroup of Ghana and some aspects of its associated gold mineralization. Precambrian Research 46, 139–165.

Loh, G., Hirdes, W., Anani, C., Davis, D.W., Vetter, U., 1999. Explanatory notes for the geological map of Southwest Ghana 1: 100,000. Geologisches Jahrbuch B 93, 150.

MacLeod, I.N., Jones, K., Fan Dai, T., 1993. 3-D analytic signal in the interpretation of total magnetic field data at low magnetic latitudes. Exploration Geophysics 24, 679–688.

Mahar, E.M., Baker, J.M., Powell, R., Holland, T.J.B., Howell, N., 1997. The effect of Mn on mineral stability in metapelites. Journal of Metamorphic Geology 15, 223–238.

Mensah, M., 1973. On the question of the age of the Sekondi Series, upper devonian or lower carboniferous rocks of Ghana. Ghana Journal of Sciences 13, 134–139.

Metelka, V., Baratoux, L., Naba, S., Jessell, W.M., 2011. A geophysically constrained litho-structural analysis of the Eburnean greenstone belts and associated granitoid domains, western Burkina Faso. Precambrian Research 190, 48–69.

Milési, J.P., Feybesse, J.L., Pinna, P., Deschamps, Y., Kampunzu, H., Muhongo, S., Lescuyer, J.L., Le Goff, E., Delor, C., Billa, M., Ralay, F., Heinry, C., 2004. Geological map of Africa 1:10 000 000. SIGAfrique Project. <http://www.sigafrique.net>.

Milesi, J.P., Ledru, P., Ankrah, P., Johan, V., Marcoux, E., Vinchon, Ch., 1991. The metallogenic relationship between Birimian and Tarkwaian gold deposits in Ghana. Mineralium Deposita 26, 228–238.

Milési, J.P., Ledru, P., Feybesse, J.L., Dommanget, A., Marcoux, E., 1992. Early Proterozoic ore deposits and tectonics of the Birimian orogenic belt, West Africa. Precambrian Research 58, 305–344.

Milligan, P.R., Gunn, P.J., 1997. Enhancement and presentation of airborne geophysical data. AGSO Journal of Australian Geology and Geophysics 17 (2), 63–75.

Mumin, A.H., Fleet, M.E., 1995. Evolution of gold mineralization in the Ashanti Gold Belt, Ghana: evidence from carbonate compositions and parageneses. Mineralogy and Petrology 55, 265–280.

Mumin, A.H., Fleet, M.E., Chryssoulis, S.L., 1994. Gold mineralization in As-rich mesothermal gold ores of the Bogosu-Prestea mining distric of the Ashanti Gold Belt, Ghana: remobilization of invisible gold. Mineralium Deposita 29, 445–460.

Mumin, A.H., Fleet, M.E., Longstaffe, F.J., 1996. Evolution of hydrothermal fluids in the Ashanti Gold Belt, Ghana: stable isotope geochemistry of carbonates, graphite, and quartz. Economic Geology 91, 135–148.

Ntiamoah-Agyakwa, Y., 1979. Relationship between gold and manganese mineralizations in the Birimian of Ghana, West Africa. Geological Magazine 116, 345–352.

Nyame, F.K., Kase, K., Yamamoto, M., 1998. Spessartine garnets in a manganiferous carbonate formation from Nsuta, Ghana. Resource Geology 48 (1), 13–22.

Oberthür, T., Vetter, U., Davis, D.W., Amanor, J.A., 1998. Age constraints on gold mineralization and Paleoproterozoic crustal evolution in the Ashanti belt of southern Ghana. Precambrian Research 89, 129–143.

Oberthür, T., Vetter, U., Schmidt Mumm, A., Weiser, T., Amanor, J.A., Gyapong, W.A., Kumi, R., Blenkinsop, T.G., 1994. The Ashanti Gold Mine at Obuasi, Ghana: mineralogical, geochemical, stable isotope and fluid inclusion studies on the metallogenesis of the deposit. Geologisches Jahrbuch D 100, 31–129.

Oberthür, T., Weiser, T., Amanor, J.A., Chryssoulis, S.L., 1997. Mineralogical siting and distribution of gold in quartz veins and sulfide ores of the Ashanti mine and other deposits in the Ashanti belt of Ghana: genetic implications. Mineralium Deposita 32, 2–15.

Pigois, J.P., Groves, D.I., Fletcher, I.R., McNaughton, N.J., Snee, L.W., 2003. Age constraints on Tarkwaian palaeoplacer and lode-gold formation in the Tarkwa-Damang district, SW Ghana. Mineralium Deposita 38, 695–714.

Schmidt Mumm, A., Oberthür, T., Vetter, U., Blenkinsop, T.G., 1997. High CO$_2$ content of fluid inclusions in gold mineralisations in the Ashanti Belt, Ghana: a new category of ore forming fluids? Mineralium Deposita 32, 107–118.

Schwartz, M.O., Oberthür, T., Amanor, J., Gyapong, W.A., 1992. Fluid inclusion re-equilibration and P-T-X constraints on fluid evolution in the Ashanti gold deposit, Ghana. European Journal of Mineralogy 4, 1017–1033.

Sestini, G., 1973. Sedimentology of a Paleoplacer: the gold-bearing Tarkwaian of Ghana. Ores in Sediments, International Union of Geological Sciences, Series A 3, 275–305.

Taylor, P.N., Moorbath, S., Leube, A., Hirdes, W., 1992. Early Proterozoic crustal evolution in the Birimian of Ghana: constraints from geochronology and isotope geochemistry. Precambrian Research 56, 97–111.

Tevendale, W.B., 1950. Annual report 1948–49. Gold Coast Geological Survey, 32.

Tshibubudze, A., Hein, K.A.A., Marquis, P., 2009. The Markoye shear zone in NE Burkina Faso. Journal of African Earth Sciences 55, 245–256.

Tunks, A.J., Selley, D., Rogers, J.R., Brabham, G., 2004. Vein mineralization at the Damang Gold Mine, Ghana: controls on mineralization. Journal of Structural Geology 26, 1257–1273.

Talwani, M., Heirtzler, J.R., 1964. In: Parks, G.A. (Ed.), Computation of Magnetic Anomalies Caused by Two-Dimensional Bodies of Arbitrary Shape. Computers in the Mineral Industries. School of Earth Sciences, Stanford University, pp. 464–480.

Talwani, M., Worzel, J.I., Landisman, M., 1959. Rapid gravity computations for two-dimensional bodies with application to the Mendicino submarine fracture zone. Journal of Geophysical Research 64, 49–59.

Verduzco, B., Fairhead, J.D., Green, C.M., 2004. New insights into magnetic derivatives for structural mapping. The Leading Edge 29 (1), 24–29.

Whitelaw, O.A.L., 1929. The Geological and Mining Features of the Tarkwa-Abosso Goldfield. Gold Coast Geological Survey, Memoir No. 1, 46 p.

Wille, S.E., Klemd, R., 2004. Fluid inclusion studies of the Abawso gold prospect, near the Ashanti Belt, Ghana. Mineralium Deposita 39, 31–45.

Yao, Y., Murphy, P.J., Robb, L.J., 2001. Fluid characteristics of Granitoid-Hosted gold deposits in the Birimian Terrane of Ghana: a fluid inclusion microthermometric and Raman spectroscopic study. Economic Geology 96, 1611–1643.

Yao, Y., Robb, L.J., 2000. Gold mineralization in Palaeoproterozoic granitoids at Obuasi, Ashanti region, Ghana: ore geology, geochemistry and fluid characteristics. South African Journal of Geology 103, 255–278.